Project no. TIP5-CT-2006-031415

# INNOTRACK

Integrated Project (IP)

Thematic Priority 6: Sustainable Development, Global Change and Ecosystems

# D2.1.3 First phase report on the modelling of poor quality sites

Due date of deliverable: 2008/02/29

Actual submission date: 2008/07/04

Start date of project: 1 September 2006 Duration: 36 months

Organisation name:
Czech Technical University in Prague

Final

| Project co-funded by the European Commission within the Sixth Framework Programme (2002-2006) | | |
|---|---|---|
| **Dissemination Level** | | |
| **PU** | Public | X |
| **PP** | Restricted to other programme participants (including the Commission Services) | |
| **RE** | Restricted to a group specified by the consortium (including the Commission Services) | |
| **CO** | Confidential, only for members of the consortium (including the Commission Services) | |

# Table of Contents

# Table of figures

# 1. Executive Summary

In agreement with the content of partial Task 2.1.8 Physical modelling of poor quality sites of the integrated INNOTRACK project, the objective was to perform the physical modelling of substructure with a low bearing capacity of the subgrade and variable thickness of the ballast bed. The substructure was modelled in laboratory conditions in a 1:1 scale. Model constructions were loaded with forces corresponding to static axle loads of 22.5 t; 25.0 t and 27.5 t. The research objective was to determine the deflection values of the ballast layer of gravel under the sleeper and the sub-ballast layer of crushed stone mixture, to measure the values of the moduli of deformation and the impact moduli of deformation, to assess the effect of the thickness of gravel on the sleeper and sub-ballast layer deflection values and the effect of a resilient under-sleeper pad on changes in the gravel and sub-ballast layer deformations. This Deliverable also comprises the particular results of Task 2.1.10 Numerical modelling of poor quality sites.

# 2. Introduction

## 2.1 Methodology of physical modelling

A series of laboratory measurements on substructure models with dimensions of 2 x 1 x 0.8 m was performed in the experimental box of the Department of Railway Structures of the Faculty of Civil Engineering, Czech Technical University in Prague. The substructure was modelled in a 1:1 scale. In order to ensure unchangeable characteristics, the subgrade was modelled by a layer of rubber with a known bearing capacity (to simulate poor subgrade two bearing capacities were chosen expressed by the static modulus of deformation under the German methodology [1] with values of 20 MPa and 30 MPa). The subgrade was overlaid with a sub-ballast layer of crushed stone mixture with a constant thickness of 20 cm. A ballast bed with thicknesses of 25 cm, 35 cm and 45 cm was laid on the sub-ballast layer, and a half of a concrete sleeper without a resilient pad and with a resilient under-sleeper pad were mounted onto it.

## 2.2 Methodology of numerical modelling

In order to develop a new method for designing construction of subbase, using a multilayer approach, new geosynthetics or other reinforcing means, such as lime horizontal layers, or cement columns a set of Finite Element Models has been developed. To evaluate the possibilities of the models to reflect behaviour of the real construction a set of experiments using laboratory box with different design of construction layers (and later using reinforcing geosynthetics) is used and bearing capacity of the construction is assessed and compared to values obtained from the numerical simulations.

With advancement of new geosynthetics, namely reinforcing geogrids, the need for new design method emerged. The advantage of using a combined approach of laboratory experiments and numerical methods is straightforward. There exists no exact method to design construction of subbase under various geotechnical conditions and use of new materials in the construction layers makes the situation even more challenging. To use numerical modelling to solve such a complex problem is therefore essential.

The aim of this study is to show the possibilities of numerical modelling and to develop a unified approach to find an optimal solution to design the subbase for different bearing capacity required.

List of the studied models:

1. axisymmetric FE model of the experimental box
2. 3-D FE model of the experimental box
3. axisymmetric FE model of the in-situ conditions
4. 3-D FE model with reinforcing geogrid

The first two sets of models were set up according to the experimental set-up – a part of the track bed in 1:1 scale (experimental box) in which all the possible configurations are to be studied. The third model is an extension of the results to conditions of a real track. The last two groups of models consider reinforcement and special attention is paid to proper modelling of the interface between the reinforcement and respective layer.

# 3. The effect of axle load increase on the permanent way construction

## 3.1 Permanent way construction

Model measurements in the experimental box were made using a section of a part of the permanent way construction in a 1:1 scale, which was loaded with a maximum force P which acts on the half of a concrete sleeper when the rail is loaded with a wheel force Q. A diagram of the permanent way construction loaded with the wheel force is shown in Figure 1.

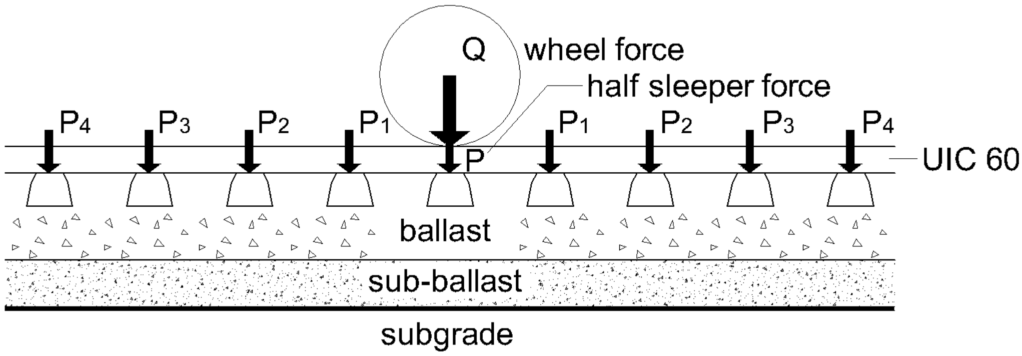


***Figure 1: Calculation diagram of model loading in the experimental box***

## 3.2 Modelling of substructure construction

In order to investigate the effect of increased axle loads on the permanent way construction, model substructure constructions consisting of a three-layer system composed of a layer of gravel under the sleeper, a sub-ballast layer of granulated layer and a layer of rubber plates simulating the subgrade soil were investigated in the experimental box (Figure 2). The substructure was loaded with a half of a concrete sleeper on which the force P was acting (Figure 3).

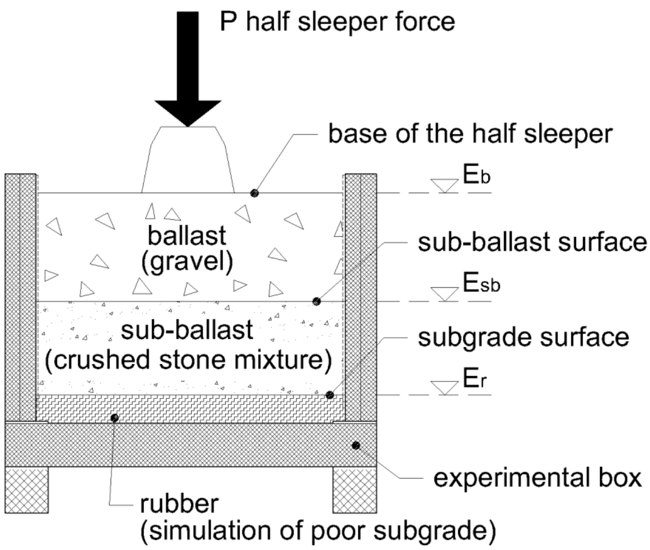


***Figure 2: Identification of parts of the permanent way model construction in the experimental box***

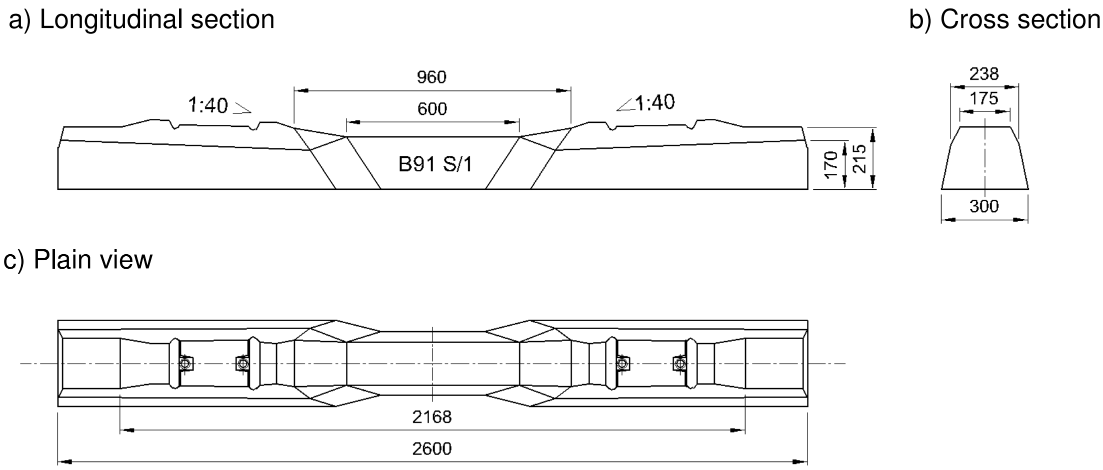


***Figure 3: Diagram of sleeper B 91 S/1, a) longitudinal section, b) cross section, c) plain view***

# 3.3 Calculation of load distribution from the rail onto the sleeper

The calculation of the load exerted onto the sleeper by the axle force was made using the calculation of a beam resting on resilient supports according to Zimmermann. The calculation considered a rail UIC 60, a sleeper B91 S/1, a distance between sleepers of 0.6 m. The quality of rail mounting was characterized by the loading capacity coefficient C.

The magnitude of the force transferred onto the loaded sleeper depends mainly on the rail shape and its wear, on the permanent way and substructure material.

In the calculation of the rail deflection (in m) at the point exposed to the load exerted by the railway vehicle wheel the following formula is used:

- Deflection in m due to static load [8] is:

$$y = \frac{Q}{2 \cdot C \cdot b \cdot L} \cdot \nu ,$$

where: Q – the static wheel force in N,

C – the loading capacity coefficient in $Pa.m^{-1}$,

$b = \frac{F}{2 \cdot a}$ in m,

F – the sleeper loading area in $m^2$,

a – the axial distance of sleepers in m,

$L = \sqrt[4]{\frac{4 \cdot E \cdot I_x}{b \cdot C}}$ in m,

E – the elastic modulus of steel ($2{,}1.10^{11}$ Pa),

$I_x$ – inertia moment in kg.m,

$E.I_x$ – the beam lateral rigidity in $N.m^2$.

$\nu = (\cos\kappa + \sin\kappa) \cdot e^{-\kappa}$ ,

$\kappa = \frac{x}{L}$ ,

x – the distance from the point of wheel force action in m.

The dynamic coefficient for the calculation of the stress exerted onto the rail due to operating load is determined in relation to the presumed substructure quality and the vehicle travel speed. Its value chosen was 1.25.

Figure 4 displays the influence line pattern of the deformation of the rail UIC 60 exposed to loading by one wheel force for various track bed qualities.

The calculation resulted in the determination of the load acting on sleepers in the percentage of the wheel force exerted by the rail onto the sleeper (Figure 5).

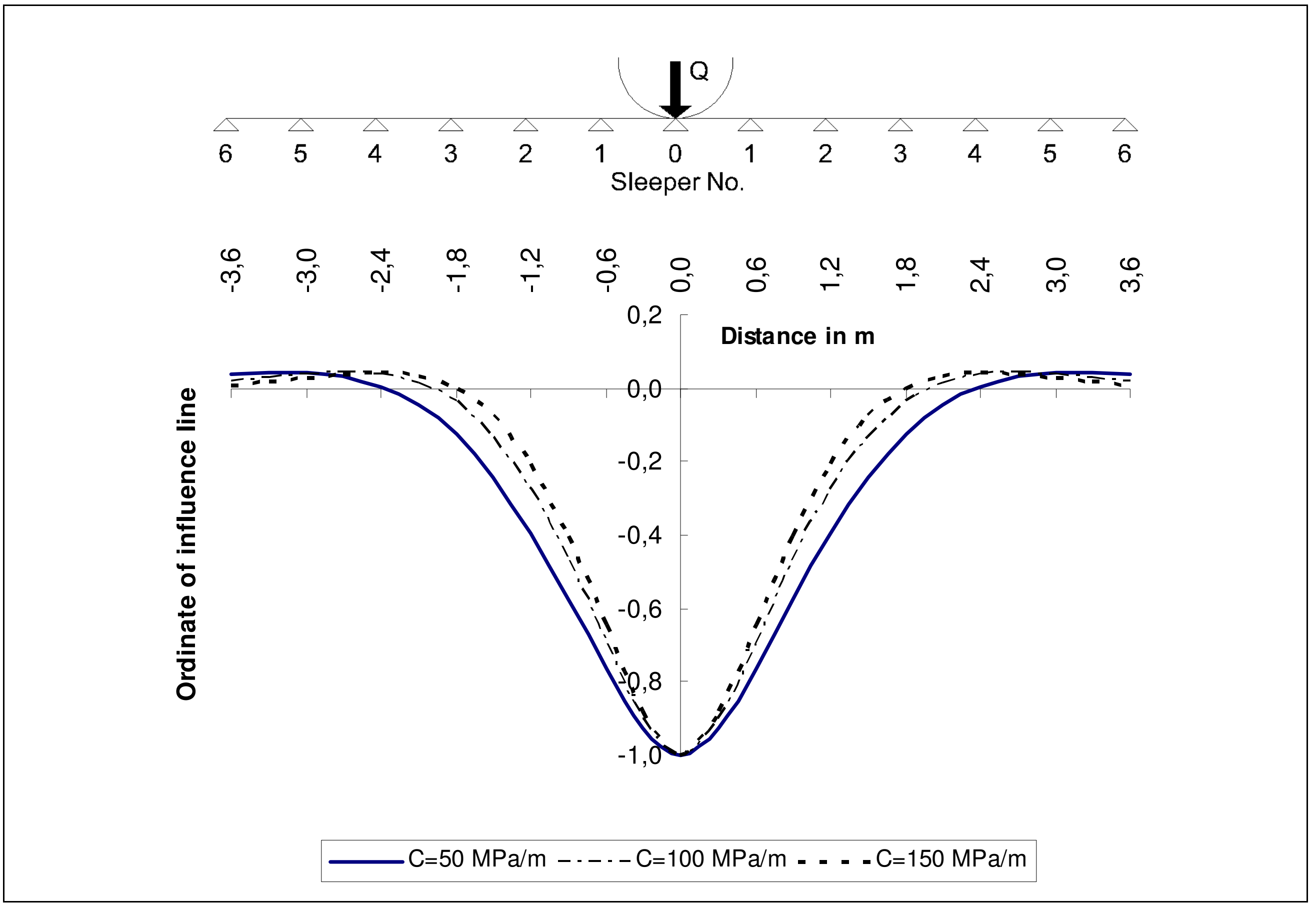


***Figure 4: Time pattern of the influence line of UIC 60 rail deformation under the load by one wheel force for substructure quality C = 50, 100 a 150 MPa.m$^{-1}$***

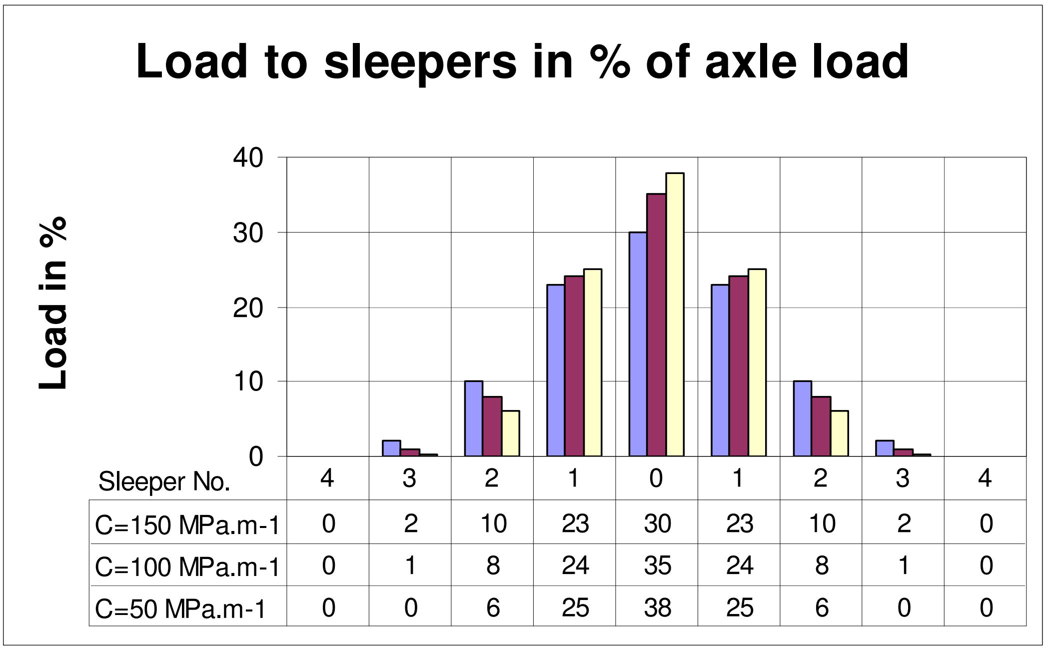


| Sleeper No. | 4 | 3 | 2 | 1 | 0 | 1 | 2 | 3 | 4 |
|---|---|---|---|---|---|---|---|---|---|
| C=150 MPa.m-1 | 0 | 2 | 10 | 23 | 30 | 23 | 10 | 2 | 0 |
| C=100 MPa.m-1 | 0 | 1 | 8 | 24 | 35 | 24 | 8 | 1 | 0 |
| C=50 MPa.m-1 | 0 | 0 | 6 | 25 | 38 | 25 | 6 | 0 | 0 |

***Figure 5: Sleeper load percentage for substructure quality C = 50, 100 a 150 MPa.m$^{-1}$ by the load the sleeper No. 0 by force P, rail UIC 60***

## 3.4 Calculation of half sleeper load for axle loads of 22.5 t, 25.0 t and 27.5 t

The calculation of the force P exerted by the rail onto the half sleeper considered the quality of the track bed expressed by the loading capacity coefficient C = 50 MPa.m$^{-1}$, the dynamic coefficient 1.25 for the travel speed v = 120-160 km.h$^{-1}$. The following forces P exerted by the rail onto the half sleeper were calculated for the investigated axle loads:

- for 2Q = 22.5 t the force calculated P = 42.00 kN,
- for 2Q = 25.0 t the force calculated P = 46.65 kN,
- for 2Q = 27.5 t the force calculated P = 51.30 kN.

The calculated values of forces P for different axle loads were used in loading the model constructions in the experimental box.

# 4. Experimental verification of axle load increase in the experimental box

## 4.1 Description of the experimental box

Model constructions of substructure were loaded in the experimental box, which was built of welded sections with removable walls of wooden baulk with a cross section of 100 x 150 mm. To minimize the friction of the model with the walls of the box, these were panelled with galvanized plate with a thickness of 0.55 mm. To enable the measurement of the moduli of deformation by means of a rigid circular plate at different levels of the substructure, a mobile load frame was designed for the load tests. The basic dimensions of the experimental box are shown in Figure 6. The experimental box with a mobile frame is seen in Figure 7.

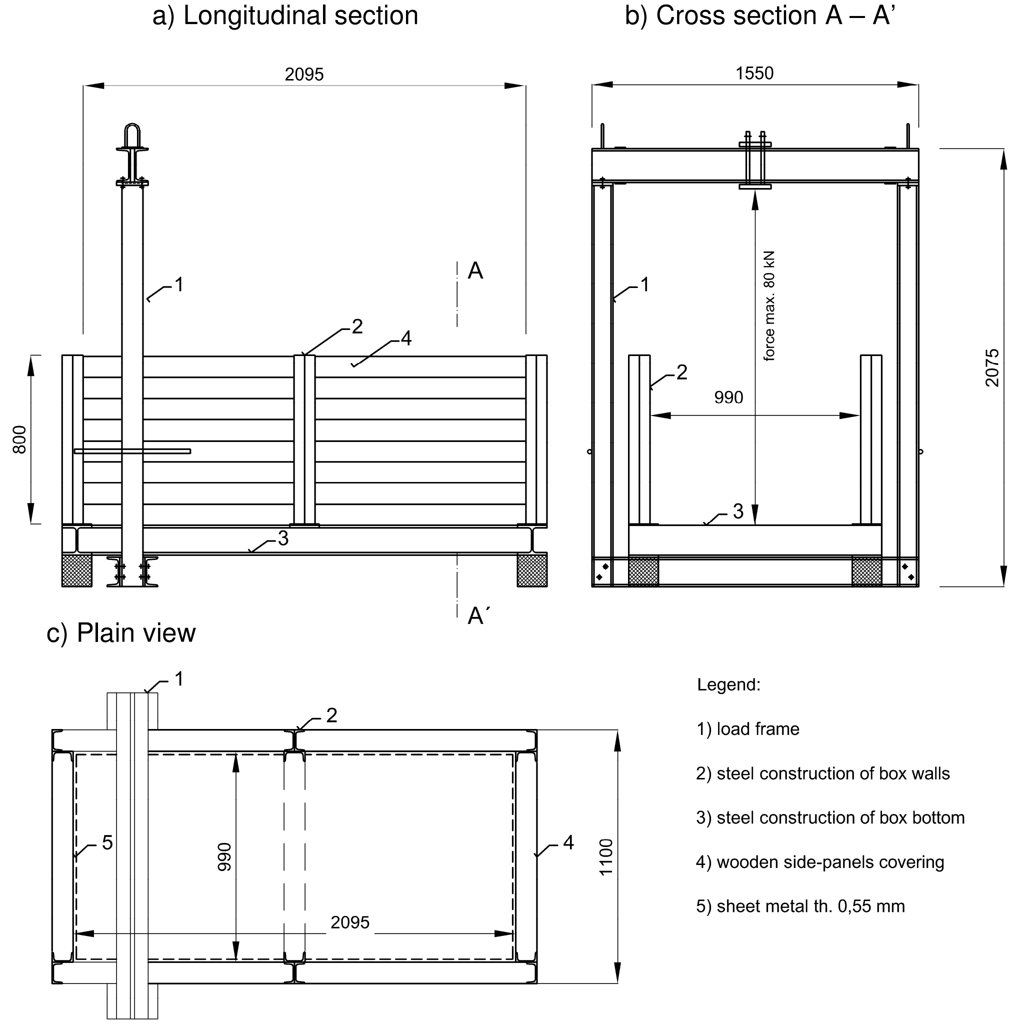


***Figure 6: Basic dimensions of the experimental box, a) longitudinal section, b) cross section A – A', c) plain view***

***Figure 7: The experimental box with a movable frame***

## 4.2 Model constructions of substructure

Model constructions of substructure were composed of three layers. The subgrade was simulated by means of rubber plates with the modulus of deformation under DIN 18 134 [1], which simulated the subgrade soil. The use of rubber plates allowed ensuring the constant bearing capacity of the subgrade for the whole time of laboratory tests. Rubber plates REMAPUR 2085 with a thickness of 23 mm, REMAPUR 2089 with a thickness of 25 mm and USM 850 with a thickness of 19 mm (total thickness of rubber plates of 67 mm) provided the following values:

- static modulus of deformation $E_{V2}$ = 20.3 MPa,
- impact modulus of deformation $E_{vd}$ = 11.3 MPa.

Rubber plates REMAPUR 2085 with a thickness of 23 mm and REMAPUR 2089 with a thickness of 25 mm (total thickness of rubber plates of 48 mm) provided the following values:

- static modulus of deformation $E_{V2}$ = 31.8 MPa,
- impact modulus of deformation $E_{vd}$ = 13.8 MPa.

To label the bearing capacity of the rubber plates simulating the subgrade, the characteristics of individual models used the symbols E20 (for bearing capacity $E_{V2}$ = 20.3 MPa) and E30 (for bearing capacity $E_{V2}$ = 31.8 MPa).

The rubber plates were overlaid with an sub-ballast of crushed stone mixture graded 0 – 32 mm with a thickness after compaction of 20 cm. The crushed stone mixture layer was compacted with a special manual vibratory compacting device with an active area of 174 x 174 mm. Compaction was performed in one layer. The compaction duration set was 30 min. evenly along the whole surface of the experimental box. The course of compaction of the layer of gravel is shown in Figure 8.

The sub-ballast of crushed stone mixture was gradually overlaid with a layer of gravel graded 32 – 63 mm in three thicknesses: 25 cm, 35 cm and 45 cm. The layer of gravel with a thickness of 25 cm was compacted in two layers with a thickness of ca 12.5 cm. When increasing the gravel thickness to 35 cm the layer increased by 10 cm was again compacted along the whole surface of the experimental box. Compaction of the 10 cm layer of gravel in increasing the thickness to 45 cm was again performed along the whole surface of the experimental box.

***Figure 8: Course of compaction of the layer of gravel***

On the surface of the layer of gravel, a half of an instrumented sleeper B 91 S/1 of pre-stressed concrete with a 50 cm long piece of rail UIC 60 was mounted. The rail was mounted on a rubber pad of WU 7 type with a thickness of 7 mm and fastened to the sleeper using fastening without soleplates with clips Vossloh SKL 14. In the first series of load tests, a half sleeper was mounted on the gravel surface without the under-sleeper pad, while in the second series of load tests a half of the concrete sleeper used was fitted at its lower surface with the under-sleeper pad Getzner SYLOMER SLS 613 with a thickness of 13 mm. The following elasticity characteristics were determined on the under-sleeper pad:

| | |
|---|---|
| Static rigidity | $C_{stat} = 0.06\ N.mm^{-3}$ |
| Modulus of deformation | $E_{V2} = 16.1$ MPa |
| Impact modulus of deformation | $E_{vd} = 17.4$ MPa |

The static rigidity and the modulus of deformation of the under-sleeper pad were determined in the hydraulic press, while the impact modulus of deformation on the concrete floor of the testing laboratory (rigid subsoil hypothesis). The half sleeper without the under-sleeper pad and with the under-sleeper pad is shown in Figure 9

a) b)

***Figure 9: Half sleeper as seen a) without the under-sleeper pad, b) with the under-sleeper pad***

Model constructions of substructure were loaded with a force P exerted by the rail on the half of a sleeper. This force was calculated for axle loads 2Q = 22.5 t to 2Q = 27.5 t (see chapter 3.4).

The diagram of model constructions of substructure is in Figure 10.

a) Model constructions with the half sleeper without the under-sleeper pad

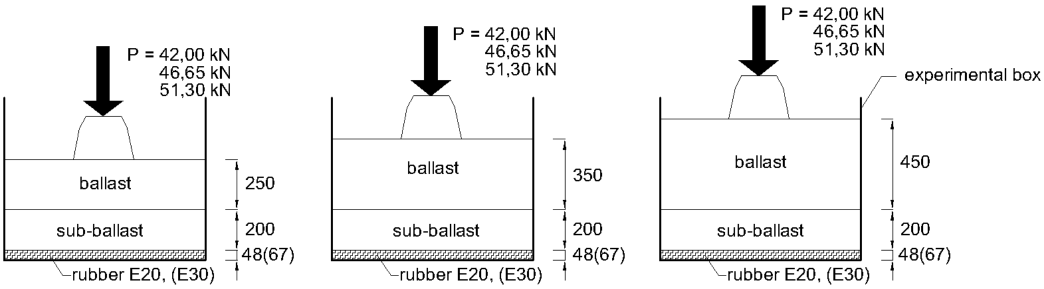


b) Model constructions with the half sleeper with the under-sleeper pad

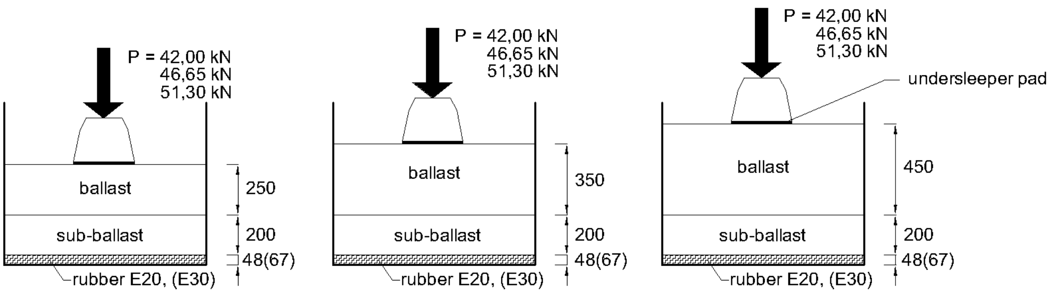


***Figure 10: Diagram of model constructions of substructure in the experimental box (variation of the load P for axle loads 2Q = 22.5 t, 2Q = 25.0 t, 2Q = 27.5 t and for 2 different bearing capacities of rubber plates simulating earth E20 and E30, a) half sleeper without the under-sleeper pad b) half sleeper with the under-sleeper pad***

With a view to the large number of tested constructions of substructure, the following symbols were selected for individual model constructions:

E.g. Model B25/SB20/E20 means:

B25 = thickness of gravel under the sleeper in cm, (ballast),

SB20 = thickness of crushed stone mixture in cm, (sub-ballast),

E20 = bearing capacity of rubber plates simulating subgrade in MPa.

When using the half sleeper with the under-sleeper pad the model symbol was complemented with the abbreviation USP (under-sleeper pad).

E.g. Model B25/SB20/E20–USP means that the half sleeper used was fitted with the under-sleeper pad.

Load tests in the experimental box were performed for 3 different constructions of substructure (with a variable thickness of gravel) laid on rubber plates with 2 different bearing capacities and loaded with a half of a concrete sleeper without and with the under-sleeper pad. In total, 12 model constructions were loaded with three different forces P, i.e. in all 36 individual cases were evaluated.

The example in Figure 11 is the construction of model B25/SB20/E20 in the experimental box.

a) Longitudinal section

b) Cross section

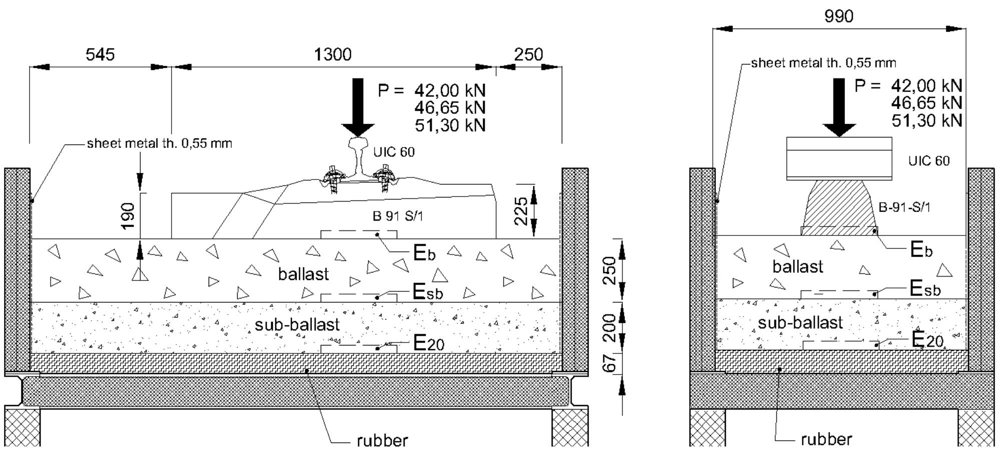


***Figure 11: Model B25/SB20/E20, a) longitudinal section, b) cross section***

# 4.3 Measurement of half sleeper deflection

In order to measure the half sleeper deflection, the upper half sleeper surface was fitted with four digital path indicators with a precision of 0.01 mm. The arrangement of the load test for the measurement of the half sleeper deflection in model B25/SB20/E20 is shown in Figure 12.

a) Longitudinal section

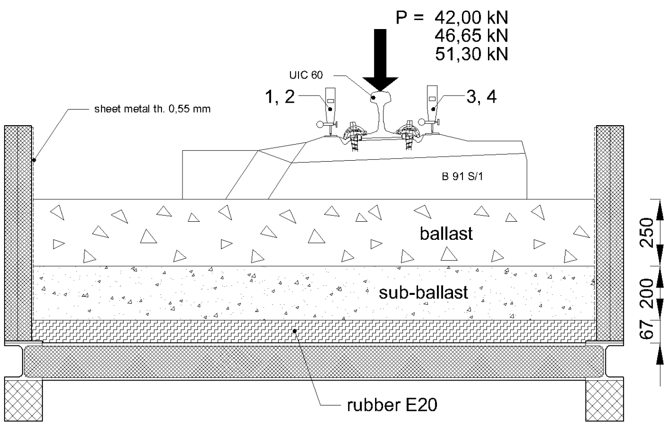

b) Plan view

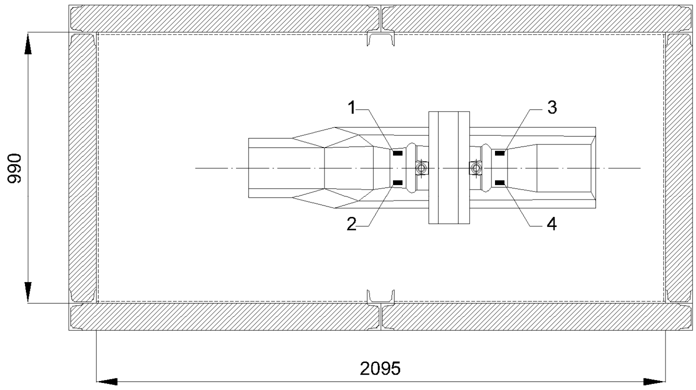


***Figure 12: Arrangement of the half of a sleeper deflection load test in model B25/SB20/E20, a) longitudinal section, b) plan view***

The objective of the load tests was to monitor the deflection of a half of the sleeper B 91 S/1 in relation to repetitive static loading of the rail head with a maximum force of 42.00 kN, 46.65 kN and 51.30 kN per half of the sleeper. First, model consolidation was carried out by repetitive loading and load relieving of the rail head in the number of 30 cycles. In each loading cycle, the rail head was loaded with the force P for a period of 1 second and successively relieved to 0 kN. The load was exerted by the manual hydraulic unit ENERPAC, which was supported on the load frame of the experimental box.

The measurement of the half sleeper deflection itself was performed in two measurement cycles of the rail head loading with the P kN = 0 kN – max P kN – 0 kN. In the third loading cycle, the rail head was gradually loaded with the force 0 kN – max P in steps by 10 kN. After reaching the maximum loading force max P kN the rail head was relieved to the value of 0 kN. The digital half sleeper deflection indicators are displayed in Figure 13.


***Figure 13: Digital indicators as seen measuring half sleeper deflection***

# 4.4 Measurement of sub-ballast deflection

To measure the deflection of the sub-ballast, its surface was fitted with 4 deflection meters. The construction of the meters is in Figure 14 and their position in Figure 15. The courses of deflections of individual indicators were monitored by means of digital path indicators with a precision of 0.01 mm. The mounting of deflection meters on the sub-ballast surface is displayed in Figure 16. A general view of deflection measurement in the experimental box is in Figure 17.

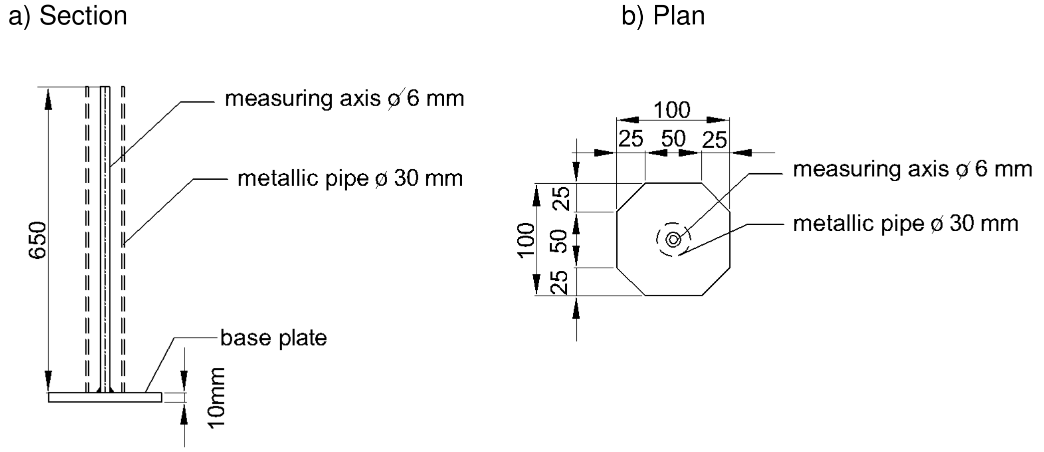


***Figure 14: Construction of deflection meter, a) section, b) plan***

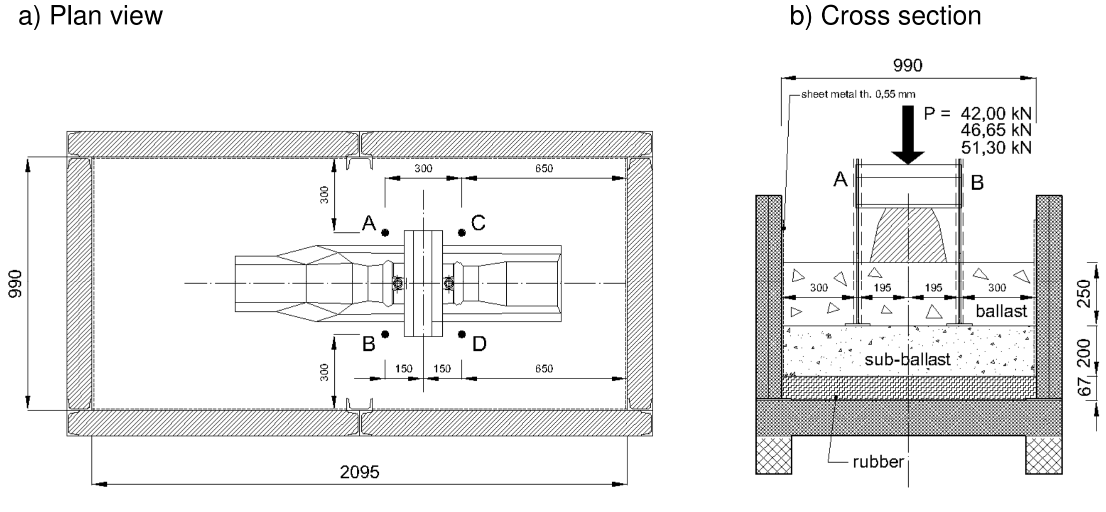


***Figure 15: Labelling and position of deflection meters in model B25/SB20/E20***

***Figure 16: Deflection meters seen mounted on the layer of crushed stone mixture***

***Figure 17: Measurement of crushed stone mixture deflection under rail head load***

## 4.5 Measurement of moduli of deformation

The objective of the measurement of the moduli of deformation was to determine the bearing capacity of individual layers of substructure. The modulus of deformation under DIN 18 134 Plattendruckversuch was determined on rubber plates, on the surface of the sub-ballast of crushed stone mixture and on the surface of the layer of gravel. The position of the load plate during the load test is clear from Figure 18. The measurement of the static modulus of deformation on the surface of the layer of gravel is seen in Figure 19. The moduli of deformation of the layer of gravel in individual models of the substructure construction were always measured after the completion of the load test and removal of the half sleeper. The moduli of deformation of the sub-ballast and rubber plates were determined during the model establishment and during its dismantling.

a) Longitudinal section

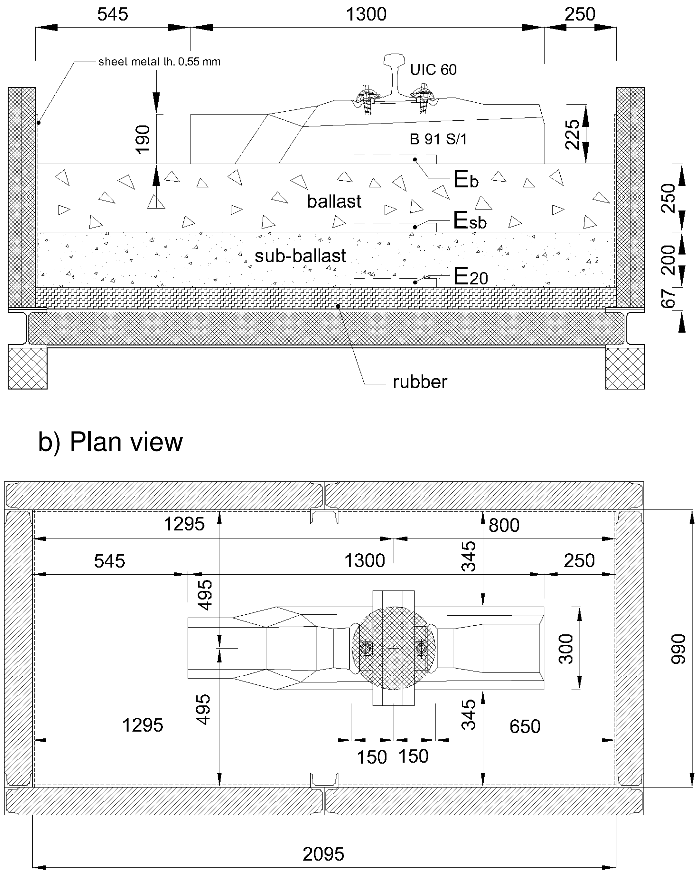


***Figure 18: Position of static load tests on model B25/SB20/E20 in the experimental box a) longitudinal section, b) plan view***

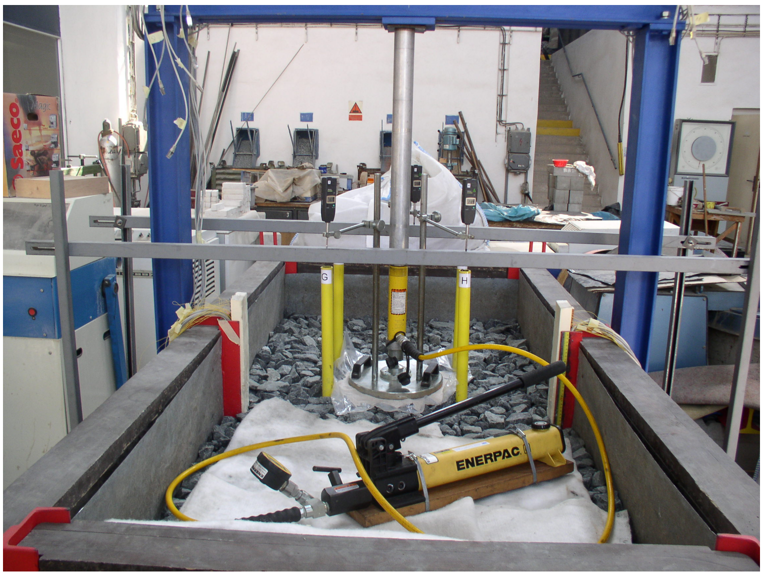


***Figure 19: Measurement of static modulus of deformation on gravel surface***

## 4.6 Measurement of impact moduli of deformation

The measurement of the impact modulus of deformation under TP BF-StB Teil B 8.3 Dynamischer Plattendruckversuch mit Leichtem Fallgewichtsgerät [2] and ČSN 73 6192 Impact Load Tests of Roads and Underlays [3] was performed with the load apparatus LDD 100 (product of firm ZBA GeoTech s.r.o, Nové Město nad Metují, Czech Republic), which consists of the guide rod on which a weight of 10 kg is moving falling from a constant height of 76.5 cm onto the impact absorber mounted on a circular rigid load plate with a diameter of 300 mm (Figure 20). The plate is fitted with the accelerometer, which allows setting the value of the plate deflection under dynamic impact. The deflection (insertion) of the load plate serves for the calculation of the impact modulus of deformation using the formula:

$$E_{vd} = \frac{F}{d \cdot s} \cdot \left(1 - \mu^2\right)$$

where: F = value of maximum impact force (7.07 kN),

μ = Poisson's ratio,

d = load plate diameter (300 mm),

s = value of elastic deflection under the load plate centre in mm.

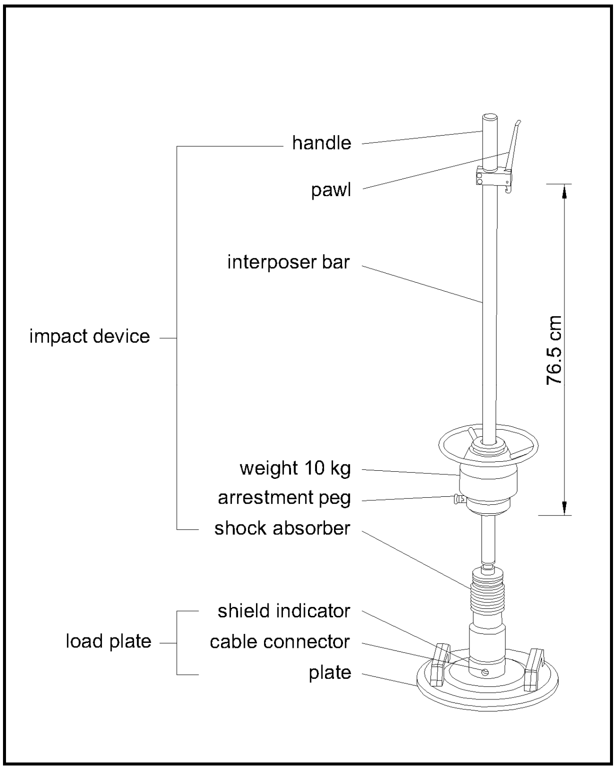


***Figure 20: Diagram of the light dynamic plate LDD 100***

Part of the load apparatus is the electronic part with the evaluation unit and a printer, which prints the protocol with three repeated measurements. The protocol shows the courses of the impact pulse, calculates the deflections of all three measurements, their mean average and the calculated value of the impact modulus of deformation $E_{vd}$. Prior to the measurement of the impact modulus of deformation, the sub-ballast under the plate was always consolidated by three impacts using a weight of 10 kg. The measurement of the impact modulus of deformation is seen in Figure 21.

a) b)

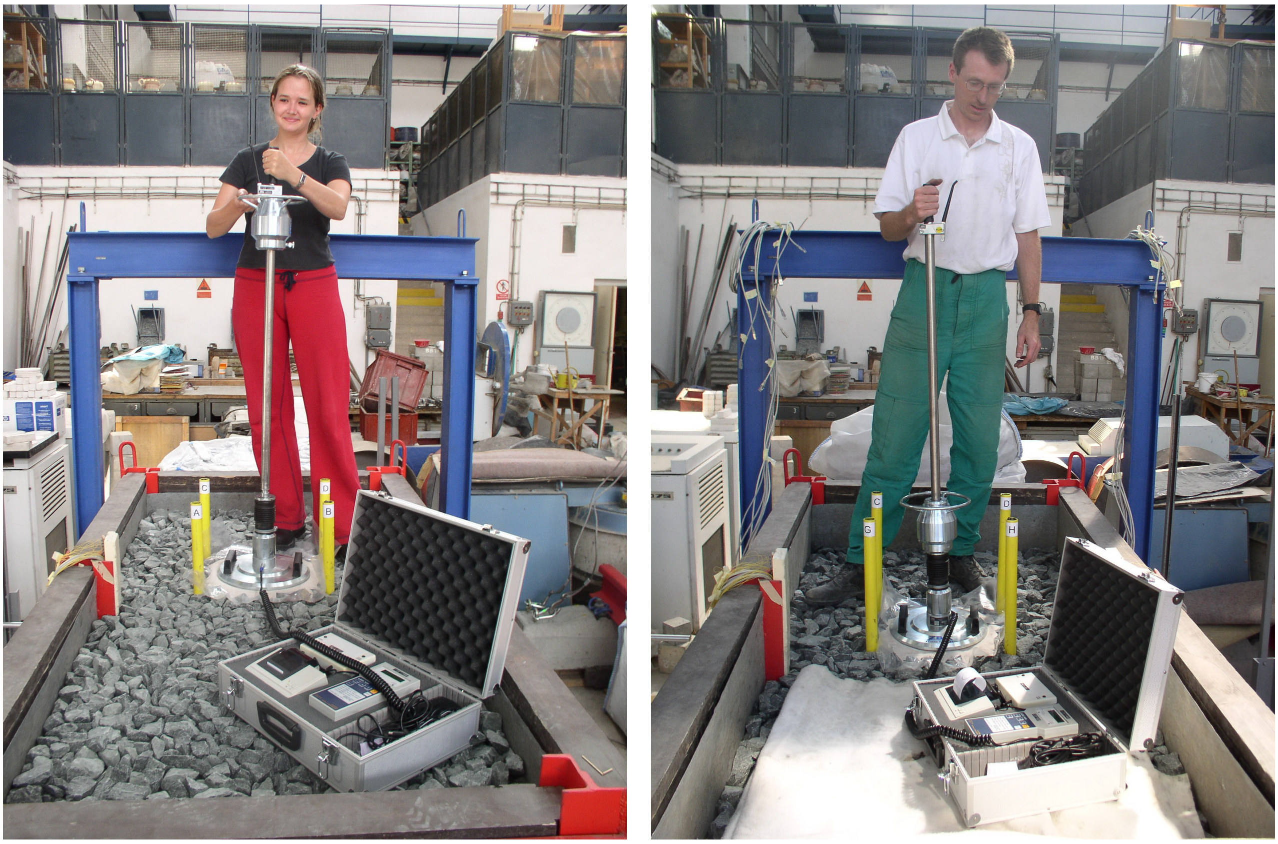

***Figure 21: Measurement with the light dynamic plate a) position of the weight before impact, b) position of the weight after the fall on the absorber***

The impact moduli of deformation of the layer of gravel in individual models of the substructure construction were always measured after the completion of the load test and removal of the half sleeper. The impact moduli of deformation of the sub-ballast and rubber plates were determined during the model establishment and during its dismantling.

## 4.7 Measurement of volume density of granulated materials

While inserting granulated materials (gravel, crushed stone mixture) inside the experimental box their density was monitored using a special digital crane scale with a precision of 0.1 kg. The known material layer thickness served for the subsequent calculation of the volume density of individual layers. After uncovering the layer of crushed stone mixture, its volume density was measured by means of the membrane volumeter, and the sample taken was used for the laboratory determination of its compaction level.

a)

b)

***Figure 22: Measurement of volume density of crushed stone mixture a) measurement with membrane volumeter, b) detail of probe***

## 4.8 Measurement of homogeneity of layers using geo-radar

For the substructure model with the greatest thickness of gravel (45 cm) geo-radar measurement was performed to assess the homogeneity of individual layers in the experimental box. At the same time, the velocity of electromagnetic waves passage through the layers and relative inductive capacity of the medium were monitored. The measurement was made with the radar apparatus SIR 20 with an aerial system of 900 Hz and 1500 MHz (Figure 23), both of these aerials acting simultaneously as a transmitter and a receiver. Both aerials measured in time steps of 0 – 20 ns. The frequency, time and method of measurement were selected to allow for probing in a depth interval of ca 0.05 to 1 m under the given conditions.

a) b)

***Figure 23: Geo-radar measurement a) with a 900 MHz aerial, b) with a 1500 MHz aerial***

The measured data was interpreted using standard procedures and software developed by GSSI Company. In order to eliminate multiple reflections and undesirable electromagnetic waves, the records were standardized into a record density of 200 scans/m.

Figure 24 shows a record from a geo-radar measurement with a 900 Hz aerial in the longitudinal and transverse direction. The measurement positions are marked as P1 and P2. The full black line represents the bottom of the box, while the dotted line the surface of gravel. The hatched area of the record was affected by nearby deflection meters.

a) b)

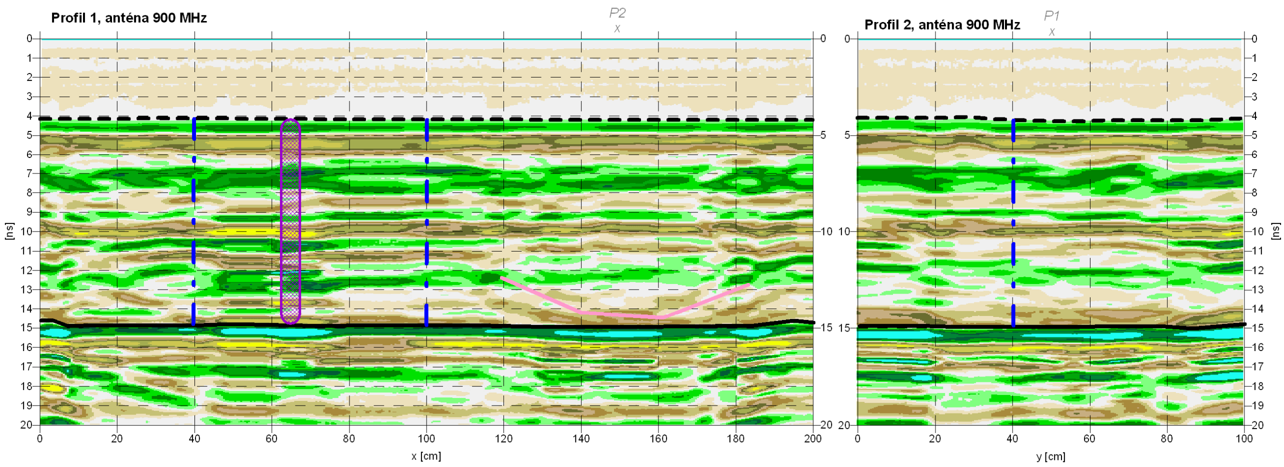


***Figure 24: Record of geo-radar measurement with a 900 Hz aerial a) longitudinal section of the experimental box, b) transverse section of the experimental box***

The time difference between the aerial and the bottom was measured as 10.9 ns, which provides - for the filler thickness of 72 cm - the resulting mean relative inductive capacity of the filler of 5.2 and the velocity of electromagnetic waves passage of 0.132 m.ns$^{-1}$. These values correspond to the expected properties of the prevailing material used (crushed amphibolite). Radar measurement was able to determine the mean characteristics of the medium inside the box, but it was beyond feasibility to distinguish in reality individual layers with similar electromagnetic properties.

## 4.9 Measurement of rubber plates deformation

In order to measure the rubber plates deformation five strain gauge rosettes RY11-3/120 (Hottinger Baldwin Messtechnik GmbH) were placed on the top surface of the rubber plate. The strain gauges were carefully glued exactly in place where the vertical displacements were measured using deflection meters. The positions were kept symmetric along the half sleeper long axis in order to enable for easy verification of the results.

From the known principal strains at selected places it is possible to calculate the vertical displacements if the deformed shape is known. To calculate the deformed shape and to establish relationship between the principal strains and vertical displacements at selected points, detailed finite element model of the experimental box was developed.

Sensitivity of the FEM model was tested in order to exclude the effects of material properties of individual layers. From the model, vertical displacements and strain components in the plane of the rubber plate were obtained and relationship between principal strain and displacement for each of the points was derived.

The relationship was used to calculate settlements of the rubber plate during the experiments based on the principal strains measured using strain gauge rosettes. This approach enables to measure not only the settlements of the half of a concrete sleeper and four selected points at the sub-ballast ballast interface but also settlements at the sub-ballast rubber interface.

## 4.9.1 Strain gauge measurements

Before laying the individual layers of the experimental box, the rubber plates simulating the soil foundation were equipped with the strain gauge rosettes. The top surface was carefully cleaned and the rosettes were carefully glued to it. The strain gauges were covered with a thin layer of fine sand as to prevent damage from crushed stones. Connecting wires were carefully placed and special care was taken to their protection.

***Figure 25: View of the strain gauge rosettes and connecting wires***

With respect to the sensitivity of strain gauges and duration of the measurement it was necessary to use the compensative strain gauge to avoid the influence of temperature. Continual measurement during the whole experiment was taken with 2 Hz sampling frequency during the static tests and 1000 Hz during dynamic tests. The experiments were performed according to DIN 18 134 and as an illustrative example a plot of principal strains measured by individual strain gauge rosettes is presented in Figure 26. The light blue dash-dot line in the bottom is strain caused by the temperature change.

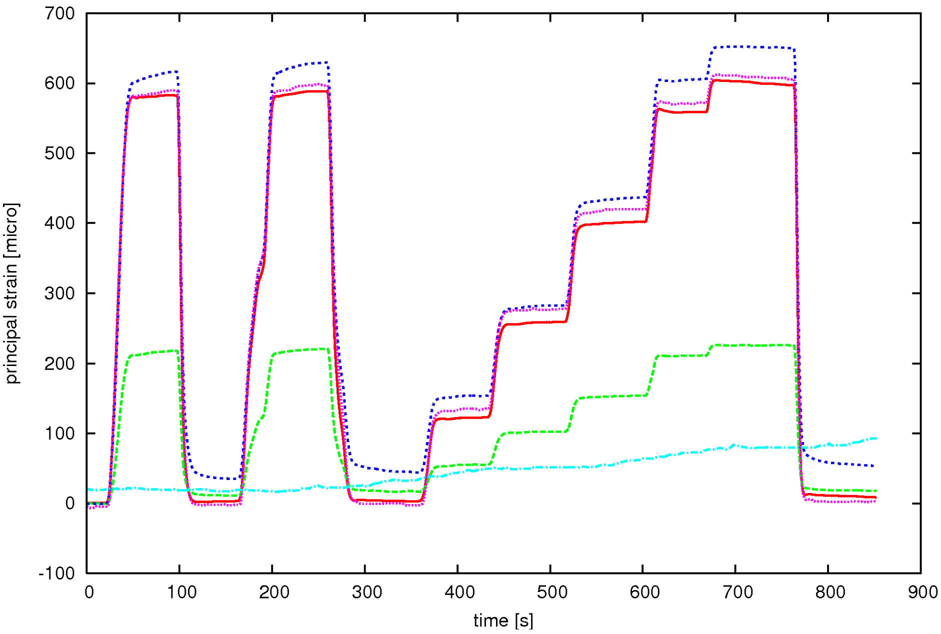


***Figure 26: Development of principal strains measured by strain gauges***

The strain development in time clearly corresponds to the applied load and show good correspondence with expected results. With the help of the FE model and resulting relationship between the principal strains and the vertical displacements at the strain gauge positions it is possible to establish the vertical displacements of the rubber plate.

# 5. Measurement on model B25/SB20/E20

## 5.1 Description of substructure construction

The construction of the substructure on which a half of a concrete sleeper B 91 S/1 without the under-sleeper pad was mounted consisted of the following layers:

- gravel (ballast) 25.0 cm
- crushed stone mixture (sub-ballast) 20.0 cm
- rubber plates 6.7 cm

The diagram of the substructure construction model B25/SB20/E20 is in Figure 11. During the establishment of the model the modulus of deformation determined on the surface of crushed stone mixture $E_{V2}$ = 37.41 MPa = $E_{sb}$ and the impact modulus of deformation $E_{vd}$ = 40.0 MPa.

## 5.2 Measurement of half sleeper deflection

The mounting position of 4 digital half sleeper deflection meters is in Figure 12. In loading the model the rail was loaded with maximum forces P = 42.0 kN – 46.65 kN – 51.3 kN, which corresponded to axle loads 2Q = 22.5 t – 25.0 t – 27.5 t. The measured maximum deflections of individual meters are in Table 1.

***Table 1: Maximum values of half sleeper deflection***

| Deflection meter | Deflection of meters in mm for rail forces | | |
|---|---|---|---|
| | **P = 42.0 kN** | **P = 46.65 kN** | **P = 51.3 kN** |
| 1 | 0.73 | 0.79 | 0.85 |
| 2 | 0.80 | 0.86 | 0.93 |
| 3 | 0.83 | 0.88 | 0.95 |
| 4 | 0.87 | 0.94 | 1.01 |
| **Mean average** | **0.81** | **0.87** | **0.94** |

The measurements of half sleeper deflections imply that the mean average values of deflections fluctuate from 0.81 mm to 0.94 mm. The measurements of deflections further imply that the values of static rigidity of the construction calculated from the formula k = P / y fluctuate from 51.9 $kN.mm^{-1}$ to 54.6 $kN.mm^{-1}$.

## 5.3 Measurement of sub-ballast deflection

The mounting position of 4 digital sub-ballast deflection meters is in Figure 13. In loading the model the rail was loaded with maximum forces P = 42.0 kN – 46.65 kN – 51.3 kN, which corresponded to axle loads 2Q = 22.5 t – 25.0 t – 27.5 t. The measured maximum deflections of individual meters are in Table 2.

***Table 2: Maximum values of sub-ballast deflection***

| **Deflection meter** | **Deflection of meters in mm for rail forces** | | |
|---|---|---|---|
| | **P = 42.0 kN** | **P = 46.65 kN** | **P = 51.3 kN** |
| A | 0.37 | 0.42 | 0.46 |
| B | 0.43 | 0.47 | 0.51 |
| C | 0.42 | 0.45 | 0.49 |
| D | 0.48 | 0.52 | 0.56 |
| **Mean average** | **0.43** | **0.47** | **0.51** |

The graphic representation of the courses of deflection of the surface of gravel and sub-ballast under the half sleeper is in Figure 27. The figure clearly shows that the deflections determined are proportional to the acting load.

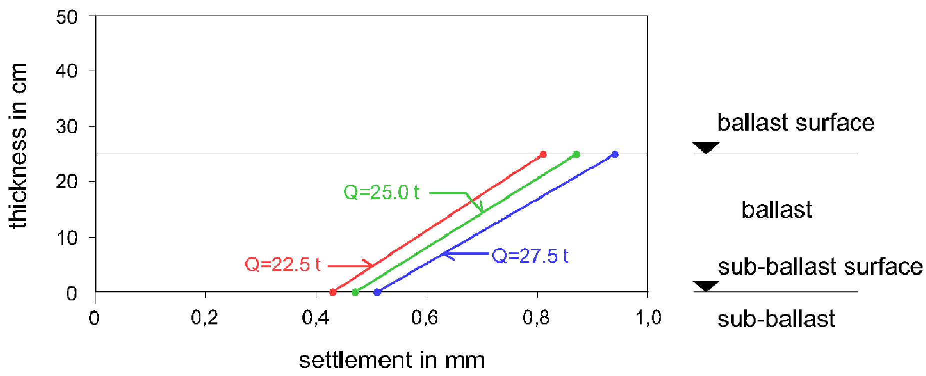


***Figure 27: Model B25/SB20/E20, graphic representation of deflection courses of the surface of gravel and half sleeper sub-ballast***

# 5.4 Measurement of moduli of deformation

The modulus of deformation of the sub-ballast layer of crushed stone mixture was measured during the model establishment. In accordance with DIN 18 134 the values determined are $E_{V1}$ = 25.7 MPa and $E_{V2}$ = 37.4 MPa = $E_{sb}$. At the same time, the ratio was calculated $E_{V2} / E_{V1}$ = 1.45.

The modulus of deformation of the surface of gravel was measured after the completion of deflection measurements and removal of the half sleeper. The measurement site of the modulus of deformation is shown in Figure 18. The values established under DIN 18 134 are $E_{V1}$ = 28.6 MPa and $E_{V2}$ = 57.1 MPa = $E_b$. Further on, the calculated ratio $E_{V2} / E_{V1}$ = 1.99.

# 5.5 Measurement of impact moduli of deformation

Impact moduli of deformation of the sub-ballast surface were determined after the measurement of the moduli of deformation of sub-ballast layer. The results of measurements of impact moduli of deformation on crushed stone mixture are in Table 3.

***Table 3: Results of measurements of impact moduli of deformation on sub-ballast***

| Load plate deflection in mm | Impact modulus of deformation $E_{vd}$ in MPa |
|---|---|
| 1.043 | 21.7 |
| 1.026 | 22.1 |
| 1.016 | 22.3 |
| **Mean average** | **22.0** |

Impact moduli of deformation of the surface of gravel were determined after the measurement of the moduli of deformation on gravel. The results of measurements of impact moduli of deformation are in Table 4.

***Table 4: Results measurements of impact moduli of deformation on gravel***

| Load plate deflection in mm | Impact modulus of deformation $E_{vd}$ in MPa |
|---|---|
| 0.529 | 42.7 |
| 0.529 | 42.7 |
| 0.516 | 43.8 |
| **Mean average** | **43.1** |

# 6. Measurement on model B25/SB20/E20–USP

## 6.1 Description of substructure construction

The construction of the substructure on which a half of a concrete sleeper B 91 S/1 with the under-sleeper pad Getzner SYLOMER SLS 613 was mounted consisted of the following layers:

- gravel (ballast) 25.0 cm
- crushed stone mixture (sub-ballast) 20.0 cm
- rubber plates 6.7 cm

The model of substructure construction B25/SB20/E20–USP is identical to model B25/SB20/E20 (see Figure 11), but the concrete half sleeper B 91 S/1 is fitted with a glued on under-sleeper pad with a thickness of 13 mm on its bottom surface. The static modulus of deformation of the under-sleeper pad determined $C_{stat} = 0.06$ N.mm$^{-3}$, the modulus of deformation $E_r = 16.1$ MPa and the impact modulus of deformation $E_{vd} = 17.4$ MPa.

In load tests with models it must be considered that in using sleepers with under-sleeper pads in long-welded rails the maximum force P acting on the sleeper will be reduced. To allow for potential comparison of the effects of the under-sleeper pad on the deflection values of the sleeper and the sub-ballast layer, the sleeper load calculated on the rail construction with sleepers with under-sleeper pads was not applied.

## 6.2 Measurement of sleeper deflection

The loading method for model B25/SB20/E20–USP is identical to that applied for model B25/SB20/E20. The half sleeper deflection again was measured at the same points of the half sleeper. The measured values of maximum deflections of individual meters mounted on the surface of the half sleeper fitted with a resilient pad are shown in Table 5.

***Table 5: Maximum values of half sleeper deflection***

| **Deflection meter** | **Deflection of meters in mm for rail forces** | | |
|---|---|---|---|
| | **P = 42.0 kN** | **P = 46.65 kN** | **P = 51.3 kN** |
| 1 | 5.15 | 5.24 | 5.34 |
| 2 | 5.20 | 5.37 | 5.51 |
| 3 | 5.17 | 5.28 | 5.45 |
| 4 | 5.23 | 5.41 | 5.62 |
| **Mean average** | **5.19** | **5.33** | **5.48** |

The measurements of half sleeper deflections imply that the mean average values of deflections fluctuate from 5.19 to 5.48 mm. The measurements of deflections further imply that the values of static rigidity of the construction calculated from the formula $k = P / y$ fluctuate from 8.1 kN.mm$^{-1}$ to 9.4 kN.mm$^{-1}$. With a view to the measured deflections the rigidity of the construction is roughly 7x lower as compared to the model B25/SB20/E20 with the half sleeper without the under-sleeper pad.

## 6.3 Measurement of sub-ballast deflection

The mounting position of deflection meters and the methods of loading the model B25/SB20/E20–USP were identical to those applied for model B25/SB20/E20. The measured values of deflections of individual meters are shown in Table 6.

***Table 6: Maximum values of sub-ballast deflection***

| Deflection meter | Deflection of meters in mm for rail forces | | |
|---|---|---|---|
| | P = 42.0 kN | P = 46.65 kN | P = 51.3 kN |
| A | 0.32 | 0.34 | 0.33 |
| B | 0.32 | 0.34 | 0.34 |
| C | 0.32 | 0.35 | 0.40 |
| D | 0.35 | 0.38 | 0.44 |
| **Mean average** | **0.33** | **0.35** | **0.38** |

The results of measurements imply that the sub-ballast deflections under variable load are practically the same.

## 6.4 Measurement of moduli of deformation

The modulus of deformation of the surface of gravel was measured after the completion of deflection measurements and removal of the half sleeper with USP. The measurement site of the modulus of deformation is shown in Figure 18. The values established under DIN 18 134 are $E_{V1}$ = 39.9 MPa and $E_{V2}$ = 64.1 MPa = $E_b$. Further on, the calculated ratio $E_{V2}$ / $E_{V1}$ = 1,61. The moduli of the sub-ballast of gravel and rubber plates were always measured during the dismantling of the model.

## 6.5 Measurement of impact moduli of deformation

Impact moduli of deformation of the surface of gravel were determined after the measurement of the moduli of deformation. The results of measurements of impact moduli of deformation are in Table 7.

***Table 7: Results measurements of impact moduli of deformation on gravel***

| Load plate deflection in mm | Impact modulus of deformation $E_{vd}$ in MPa |
|---|---|
| 0.553 | 40.9 |
| 0.550 | 41.1 |
| 0.538 | 42.0 |
| **Mean average** | **41.3** |

# 7. Measurement on model B35/SB20/E20

## 7.1 Description of substructure construction

The construction of the substructure on which a half of a concrete sleeper B 91 S/1 without the under-sleeper pad was mounted consisted of the following layers:

- gravel (ballast) 35.0 cm
- crushed stone mixture (sub-ballast) 20.0 cm
- rubber plates 6.7 cm

The diagram of the substructure construction model B35/SB20/E20 is in Figure 28. During the establishment of the model the modulus of deformation determined on the surface of crushed stone mixture $E_{V2}$ = 37.4 MPa = $E_{sb}$ and the impact modulus of deformation $E_{vd}$ = 40.0 MPa.

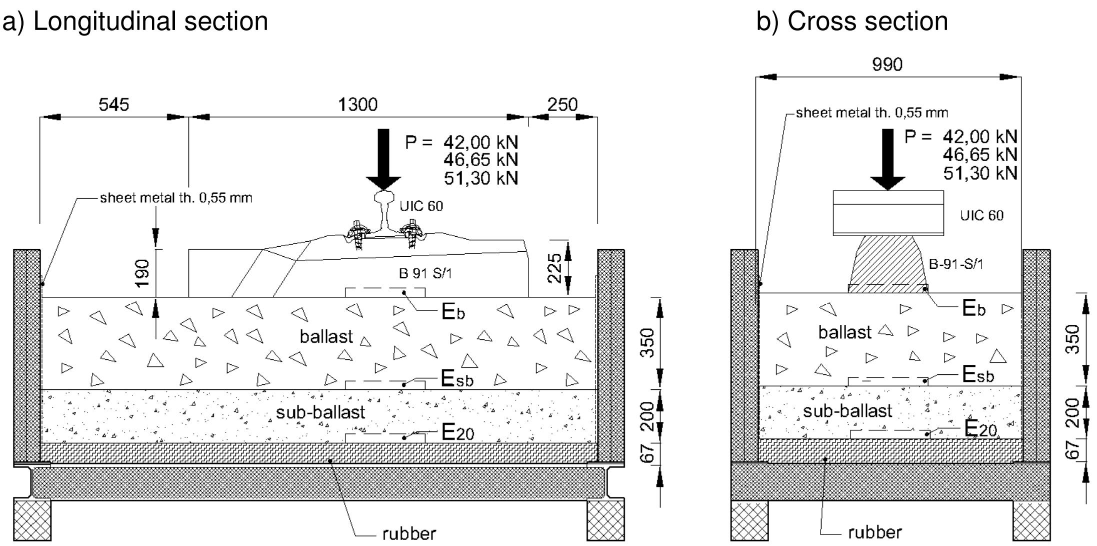


***Figure 28: Model B35/SB20/E20, a) longitudinal section, b) cross section***

## 7.2 Measurement of half sleeper deflection

The mounting position of 4 digital half sleeper deflection meters is in Figure 12. In loading the model the rail was loaded with maximum forces P = 42.0 kN – 46.65 kN – 51.3 kN, which corresponded to axle loads 2Q = 22.5 t – 25.0 t – 27.5 t. The measured maximum deflections of individual meters are in Table 8.

***Table 8: Maximum values of half sleeper deflection***

| **Deflection meter** | **Deflection of meters in mm for rail forces** | | |
|---|---|---|---|
| | **P = 42.0 kN** | **P = 46.65 kN** | **P = 51.3 kN** |
| 1 | 0.55 | 0.59 | 0.66 |
| 2 | 0.55 | 0.60 | 0.67 |
| 3 | 0.65 | 0.71 | 0.76 |
| 4 | 0.64 | 0.69 | 0.75 |
| **Mean average** | **0.60** | **0.65** | **0.71** |

The measurements of half sleeper deflections imply that the mean average values of deflections fluctuate from 0.60 mm to 0.71 mm. The measurements of deflections further imply that the values of static rigidity of the construction calculated from the formula k = P / y fluctuate from 70.0 $kN.mm^{-1}$ to 72.3 $kN.mm^{-1}$.

## 7.3 Measurement of sub-ballast deflection

The mounting position of 4 digital sub-ballast deflection meters is in Figure 15. In loading the model the rail was loaded with maximum forces P = 42.0 kN – 46.65 kN – 51.3 kN, which corresponded to axle loads 2Q = 22.5 t – 25.0 t – 27.5 t. The measured maximum deflections of individual meters are in Table 9: Maximum values of sub-ballast deflection. The measured values do not include the deflection of the experimental box structure. The measurement results show that the deflection values of the sub-ballast layer are practically the same for different loads.

***Table 9: Maximum values of sub-ballast deflection***

| **Deflection meter** | **Deflection of meters in mm for rail forces** | | |
|---|---|---|---|
| | **P = 42.0 kN** | **P = 46.65 kN** | **P = 51.3 kN** |
| A | 0.11 | 0.13 | 0.17 |
| B | 0.13 | 0.16 | 0.21 |
| C | 0.23 | 0.25 | 0.28 |
| D | 0.21 | 0.24 | 0.26 |
| **Mean average** | **0.17** | **0.20** | **0.23** |

The graphic representation of the courses of deflection of the surface of gravel and sub-ballast under the half sleeper is in Figure 29. The figure clearly shows that the deflections determined are proportional to the acting load.

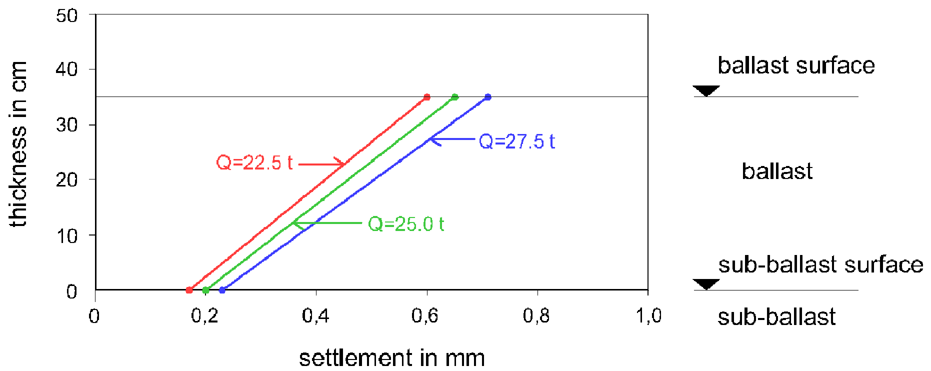


***Figure 29: Model B35/SB20/E20, graphic representation of deflection courses of the surface of gravel and half sleeper sub-ballast***

## 7.4 Measurement of moduli of deformation

The modulus of deformation of the surface of gravel was measured after the completion of deflection measurements and removal of the half sleeper. The measurement site of the modulus of deformation is shown in Figure 15. The values established under DIN 18 134 are $E_{V1}$ = 52.0 MPa and $E_{V2}$ = 105.1 MPa = $E_b$. Further on, the calculated ratio $E_{V2}$ / $E_{V1}$ = 2.02. The moduli of the sub-ballast layer of crushed stone mixture and rubber plates were measured during the dismantling of the model.

## 7.5 Measurement of impact moduli of deformation

Impact moduli of deformation of the surface of gravel were determined after the measurement of the moduli of deformation on gravel. The results of measurements of impact moduli of deformation are in Table 10.

***Table 10: Results of measurements of impact moduli of deformation on gravel***

| Load plate deflection in mm | Impact modulus of deformation $E_{vd}$ in MPa |
|---|---|
| 0.387 | 58.4 |
| 0.380 | 59.5 |
| 0.358 | 63.2 |
| **Mean average** | **60.4** |

# 8. Measurement on model B35/SB20/E20–USP

## 8.1 Description of substructure construction

The construction of the substructure on which a half of a concrete sleeper B 91 S/1 with the under-sleeper pad Getzner SYLOMER SLS 613 was mounted consisted of the following layers:

- gravel (ballast) 35.0 cm
- crushed stone mixture (sub-ballast) 20.0 cm
- rubber plates 6.7 cm

The model of substructure construction B35/SB20/E20–USP is identical to model B35/SB20/E20 (see Figure 28), but the concrete half sleeper B 91 S/1 is fitted with a glued on under-sleeper pad with a thickness of 13 mm on its bottom surface. The static modulus of deformation of the under-sleeper pad determined $C_{stat} = 0.06$ N.mm$^{-3}$, the modulus of deformation $E_r = 16.1$ MPa and the impact modulus of deformation $E_{vd} = 17.4$ MPa.

In load tests with models it must be considered that in using sleepers with under-sleeper pads in long-welded rails the maximum force P acting on the sleeper will be reduced.

## 8.2 Measurement of half sleeper deflection

The loading method for model B35/SB20/E20–USP is identical to that applied for model B35/SB20/E20. The half sleeper deflection again was measured at the same points of the half sleeper. The measured values of maximum deflections of individual meters mounted on the surface of the half sleeper fitted with a resilient pad are shown in Table 11.

***Table 11: Maximum values of half sleeper deflection***

| **Deflection meter** | **Deflection of meters in mm for rail forces** | | |
|---|---|---|---|
| | **P = 42.0 kN** | **P = 46.65 kN** | **P = 51.3 kN** |
| 1 | 5.00 | 5.21 | 5.28 |
| 2 | 4.95 | 5.18 | 5.31 |
| 3 | 5.20 | 5.40 | 5.45 |
| 4 | 5.15 | 5.38 | 5.48 |
| **Mean average** | **5.08** | **5.29** | **5.38** |

The measurements of half sleeper deflections imply that the mean average values of deflections fluctuate from 5.08 to 5.38 mm. The measurements of deflections further imply that the values of static rigidity of the construction calculated from the formula $k = P / y$ fluctuate from 8.3 kN.mm$^{-1}$ to 9.5 kN.mm$^{-1}$. With a view to the measured deflections the rigidity of the construction is roughly 10x lower as compared to the model B35/SB20/E20 with the half sleeper without the under-sleeper pad.

## 8.3 Measurement of sub-ballast deflection

The mounting position of deflection meters and the methods of loading the model B35/SB20/E20–USP were identical to those applied for model B35/SB20/E20. The measured values of deflections of individual meters are shown in Table 12. The measured values do not include the deflection of the experimental box structure.

The measurement results show that the deflection values of the sub-ballast layer are practically the same for different loads.

***Table 12: Maximum values of sub-ballast deflection***

| **Deflection meter** | **Deflection of meters in mm for rail forces** | | |
|---|---|---|---|
| | **P = 42.0 kN** | **P = 46.65 kN** | **P = 51.3 kN** |
| A | 0.18 | 0.19 | 0.21 |
| B | 0.16 | 0.17 | 0.19 |
| C | 0.25 | 0.27 | 0.30 |
| D | 0.22 | 0.25 | 0.28 |
| **Mean average** | **0.20** | **0.22** | **0.25** |

## 8.4 Measurement of moduli of deformation

The modulus of deformation of the surface of gravel was measured after the completion of deflection measurements and removal of the half sleeper with USP. The measurement site of the modulus of deformation is shown in Figure 18. The values established under DIN 18 134 are $E_{V1}$ = 63.8 MPa and $E_{V2}$ = 104.7 MPa = $E_b$. Further on, the calculated ratio $E_{V2}$ / $E_{V1}$ = 1,64. The moduli of the sub-ballast of gravel and rubber plates were always measured during the dismantling of the model.

## 8.5 Measurement of impact moduli of deformation

Impact moduli of deformation of the surface of gravel were determined after the measurement of the moduli of deformation. The results of measurements of impact moduli of deformation are in Table 13.

***Table 13: Results measurements of impact moduli of deformation on gravel***

| **Load plate deflection in mm** | **Impact modulus of deformation $E_{vd}$ in MPa** |
|---|---|
| 0.333 | 67.9 |
| 0.341 | 66.3 |
| 0.356 | 63.5 |
| **Mean average** | **65.9** |

# 9. Measurement on model B45/SB20/E20

## 9.1 Description of substructure construction

The construction of the substructure on which a half of a concrete sleeper B 91 S/1 without the under-sleeper pad was mounted consisted of the following layers:

- gravel (ballast) 45.0 cm
- crushed stone mixture (sub-ballast) 20.0 cm
- rubber plates 6.7 cm

The diagram of the substructure construction model B45/SB20/E20 is in Figure 30. During the establishment of the model the modulus of deformation determined on the surface of crushed stone mixture $E_{V2}$ = 37.4 MPa = $E_{sb}$ and the impact modulus of deformation $E_{vd}$ = 40.0 MPa.

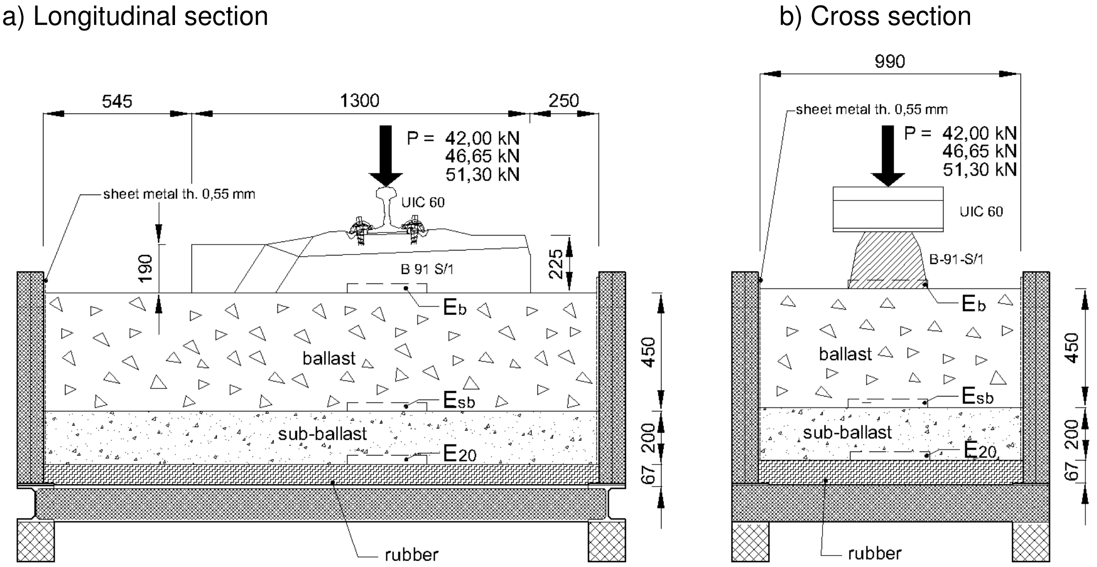


*Figure 30: Model B45/SB20/E20, a) longitudinal section, b) cross section*

## 9.2 Measurement of half sleeper deflection

The mounting position of 4 digital half sleeper deflection meters is in Figure 12. In loading the model the rail was loaded with maximum forces P = 42.0 kN – 46.65 kN – 51.3 kN, which corresponded to axle loads 2Q = 22.5 t – 25.0 t – 27.5 t. The measured maximum deflections of individual meters are in Table 14.

***Table 14: Maximum values of half sleeper deflection***

| Deflection meter | Deflection of meters in mm for rail forces | | |
|---|---|---|---|
| | **P = 42.0 kN** | **P = 46.65 kN** | **P = 51.3 kN** |
| 1 | 0.63 | 0.69 | 0.76 |
| 2 | 0.67 | 0.72 | 0.79 |
| 3 | 0.77 | 0.84 | 0.93 |
| 4 | 0.79 | 0.86 | 0.95 |
| **Mean average** | **0.72** | **0.78** | **0.86** |

The measurements of half sleeper deflections imply that the mean average values of deflections fluctuate from 0.72 mm to 0.86 mm. The measurements of deflections further imply that the values of static rigidity of the construction calculated from the formula k = P / y fluctuate from 58.3 $kN.mm^{-1}$ to 59.7 $kN.mm^{-1}$.

# 9.3 Measurement of sub-ballast deflection

The mounting position of 4 digital sub-ballast deflection meters is in Figure 15. In loading the model the rail was loaded with maximum forces P = 42.0 kN – 46.65 kN – 51.3 kN, which corresponded to axle loads 2Q = 22.5 t – 25.0 t – 27.5 t. The measured maximum deflections of individual meters are in Table 15.

***Table 15: Maximum values of sub-ballast deflection***

| Deflection meter | Deflection of meters in mm for rail forces | | |
|---|---|---|---|
| | **P = 42.0 kN** | **P = 46.65 kN** | **P = 51.3 kN** |
| A | 0.30 | 0.34 | 0.38 |
| B | 0.36 | 0.40 | 0.45 |
| C | 0.32 | 0.35 | 0.38 |
| D | 0.33 | 0.36 | 0.41 |
| **Mean average** | **0.33** | **0.36** | **0.41** |

The graphic representation of the courses of deflection of the surface of gravel and sub-ballast under the half sleeper is in Figure 31. The figure clearly shows that the deflections determined are proportional to the acting load.

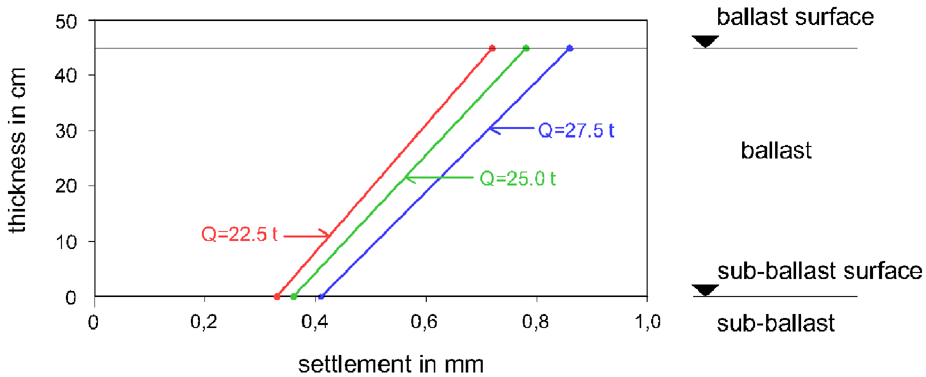


***Figure 31: Model B45/SB20/E20, graphic representation of deflection courses of the surface of gravel and half sleeper sub-ballast***

## 9.4 Measurement of moduli of deformation

The modulus of deformation of the surface of gravel was measured after the completion of deflection measurements and removal of the half sleeper. The measurement site of the modulus of deformation is shown in Figure 18. The values established under DIN 18 134 are $E_{V1}$ = 39.2 MPa and $E_{V2}$ = 117.1 MPa = $E_b$. Further on, the calculated ratio $E_{V2}$ / $E_{V1}$ = 2.99. The moduli of the sub-ballast layer of crushed stone mixture and rubber plates were measured during the dismantling of the model.

## 9.5 Measurement of impact moduli of deformation

Impact moduli of deformation of the surface of gravel were determined after the measurement of the moduli of deformation on gravel. The results of measurements of impact moduli of deformation are in Table 16.

***Table 16: Results of measurements of impact moduli of deformation on gravel***

| **Load plate deflection in mm** | **Impact modulus of deformation $E_{vd}$ in MPa** |
|---|---|
| 0.369 | 61.3 |
| 0.371 | 60.9 |
| 0.358 | 63.2 |
| **Mean average** | **61.8** |

# 10. Measurement on model B45/SB20/E20–USP

## 10.1 Description of substructure construction

The construction of the substructure on which a half of a concrete sleeper B 91 S/1 with the under-sleeper pad Getzner SYLOMER SLS 613 was mounted consisted of the following layers:

- gravel (ballast) 45.0 cm
- crushed stone mixture (sub-ballast) 20.0 cm
- rubber plates 6.7 cm

The model of substructure construction B45/SB20/E20–USP is identical to model B45/SB20/E20 (see Figure 30), but the concrete half sleeper B 91 S/1 is fitted with a glued on under-sleeper pad with a thickness of 13 mm on its bottom surface. The static modulus of deformation of the under-sleeper pad determined $C_{stat}$ = 0.06 N.mm$^{-3}$, the modulus of deformation $E_r$ = 16.1 MPa and the impact modulus of deformation $E_{vd}$ = 17.4 MPa.

In load tests with models it must be considered that in using sleepers with under-sleeper pads in long-welded rails the maximum force P acting on the sleeper will be reduced.

## 10.2 Measurement of half sleeper deflection

The loading method for model B45/SB20/E20–USP is identical to that applied for model B45/SB20/E20. The half sleeper deflection again was measured at the same points of the half sleeper. The measured values of maximum deflections of individual meters mounted on the surface of the half sleeper fitted with a resilient pad are shown in Table 17.

***Table 17: Maximum values of half sleeper deflection***

| **Deflection meter** | **Deflection of meters in mm for rail forces** | | |
|---|---|---|---|
| | **P = 42.0 kN** | **P = 46.65 kN** | **P = 51.3 kN** |
| 1 | 5.03 | 5.17 | 5.33 |
| 2 | 4.70 | 4.83 | 5.00 |
| 3 | 5.28 | 5.41 | 5.56 |
| 4 | 4.94 | 5.08 | 5.23 |
| **Mean average** | **4.99** | **5.12** | **5.28** |

The measurements of half sleeper deflections imply that the mean average values of deflections fluctuate from 4.99 to 5.28 mm. The measurements of deflections further imply that the values of static rigidity of the construction calculated from the formula k = P / y fluctuate from 8.4 kN.mm$^{-1}$ to 9.7 kN.mm$^{-1}$. With a view to the measured deflections the rigidity of the construction is roughly 7x lower as compared to the model B45/SB20/E20 with the half sleeper without the under-sleeper pad.

## 10.3 Measurement of sub-ballast deflection

The mounting position of deflection meters and the methods of loading the model B45/SB20/E20–USP were identical to those applied for model B45/SB20/E20. The measured values of deflections of individual meters are shown in Table 18. The measured values do not include the deflection of the experimental box structure.

The measurement results show that the deflection values of the sub-ballast layer are practically the same for different loads.

***Table 18: Maximum values of sub-ballast deflection***

| **Deflection meter** | **Deflection of meters in mm for rail forces** | | |
|---|---|---|---|
| | **P = 42.0 kN** | **P = 46.65 kN** | **P = 51.3 kN** |
| A | 0.16 | 0.17 | 0.19 |
| B | 0.16 | 0.17 | 0.20 |
| C | 0.17 | 0.19 | 0.22 |
| D | 0.19 | 0.22 | 0.24 |
| **Mean average** | **0.17** | **0.19** | **0.21** |

# 10.4 Measurement of moduli of deformation

The modulus of deformation of the surface of gravel was measured after the completion of deflection measurements and removal of the half sleeper with USP. The measurement site of the modulus of deformation is shown in Figure 18. The values established under DIN 18 134 are $E_{V1}$ = 64.0 MPa and $E_{V2}$ = 126.9 MPa = $E_b$. Further on, the calculated ratio $E_{V2}$ / $E_{V1}$ = 1,98.

The moduli of deformation of the sub-ballast layer surface of crushed stone mixture and rubber plates were measured during the dismantling of the model. The values determined on the layer of crushed stone mixture are $E_{V1}$ = 34.0 MPa, $E_{V2}$ = 46.1 MPa = $E_{sb}$ and the ratio $E_{V2}$ / $E_{V1}$ = 1.36. The values determined on rubber plates are $E_{V1}$ = 20.5 MPa, $E_{V2}$ = 19.6 MPa = $E_{sb}$ and the ratio $E_{V2}$ / $E_{V1}$ = 0.95.

# 10.5 Measurement of impact moduli of deformation

Impact moduli of deformation of the surface of gravel were determined after the measurement of the moduli of deformation. The results of measurements of impact moduli of deformation are in Table 19.

***Table 19: Results measurements of impact moduli of deformation on gravel***

| **Load plate deflection in mm** | **Impact modulus of deformation $E_{vd}$ in MPa** |
|---|---|
| 0.439 | 51.5 |
| 0.428 | 52.8 |
| 0.404 | 53.3 |
| **Mean average** | **52.5** |

The impact moduli of deformation of the surface of the sub-ballast layer of crushed stone mixture were verified after the measurement of the moduli of deformation on the surface of the sub-ballast layer during the dismantling of the model. The results of impact moduli of deformation measured on crushed stone mixture are displayed in Table 20.

***Table 20: Results of measurements of impact moduli of deformation on sub-ballast***

| **Load plate deflection in mm** | **Impact modulus of deformation $E_{vd}$ in MPa** |
|---|---|
| 0.789 | 28.7 |
| 0.793 | 28.5 |
| 0.780 | 29.0 |
| **Mean average** | **28.7** |

During the dismantling of the model the impact modulus of deformation of rubber plates was also determined for reference purposes. The mean value measured was $E_{vd}$ = 12.7 MPa.

# 11. Evaluation of results of experimental measurements on substructure models with a bearing capacity of simulated subgrade EV2 = 20.3 MPa

The results of experimental measurements on substructure models with a bearing capacity of subgrade E20 (with the modulus of deformation $E_{V2}$ = 20.3 MPa) lead to the following conclusions:

1. Experimental measurement on substructure models confirmed that the chosen methodology is suitable for the determination of monitored characteristics of individual substructure models where the rail was loaded with a variable force P.
2. Total results of half sleeper deflection values measured on models with a half sleeper without a resilient under-sleeper pad (models B25/SB20/E20, B35/SB20/E20, B45/SB20/E20) are displayed in Table 21.

***Table 21: Half sleeper deflection values on models with a half sleeper without a resilient under-sleeper pad***

| Ballast thickness in cm | Deflection of half sleeper in mm for rail forces | | |
|---|---|---|---|
| | **P = 42.0 kN** | **P = 46.65 kN** | **P = 51.3 kN** |
| 25 | 0.81 | 0.87 | 0.94 |
| 35 | 0.60 | 0.65 | 0.71 |
| 45 | 0.72 | 0.78 | 0.86 |
| **Mean average** | **0.71** | **0.79** | **0.83** |

In measurements on models with a half sleeper without an under-sleeper pad performed under increased axle loads from 22.5 t to 25.0 t, or 27.5 t respectively, increased half sleeper deflection occurs (half sleeper deflection for a load of 22.5 t being 100 %):

- for gravel thickness of 25 cm by 7.4 %, or 16.0 % respectively,
- for gravel thickness of 35 cm by 8.3 %, or 18.3 % respectively,
- for gravel thickness of 45 cm by 8.3 %, or 19.4 % respectively.

In increasing the axle load from 22.5 t to 25.0 t or 27.5 t, the load increase amounts to 11 % or 22 % (the load of 22.5 t being 100 %).

The lower deflection of half sleeper in case of model with 35 cm ballast thickness has not been unambiguously explained.

3. Total results of half sleeper deflection values measured on models with a half sleeper with a resilient under-sleeper pad (models B25/SB20/E20–USP, B35/SB20/E20–USP, B45/SB20/E20–USP) are displayed in Table 22.

***Table 22: Half sleeper deflection values on models with a half sleeper with a resilient under-sleeper pad***

| Ballast thickness in cm | Deflection of half sleeper in mm for rail forces | | |
|---|---|---|---|
| | **P = 42.0 kN** | **P = 46.65 kN** | **P = 51.3 kN** |
| 25 | 5.19 | 5.33 | 5.48 |
| 35 | 5.08 | 5.29 | 5.38 |
| 45 | 4.99 | 5.12 | 5.28 |
| **Mean average** | **5.08** | **5.24** | **5.38** |

In measurements on models with a half sleeper with a resilient under-sleeper pad performed under increased axle loads from 22.5 t to 25.0 t, or 27.5 t respectively, increased half sleeper deflection occurs (half sleeper deflection for a load of 22.5 t being 100 %):

- for gravel thickness of 25 cm by 2.6 %, or 5.5 % respectively,
- for gravel thickness of 35 cm by 4.1 %, or 5.9 % respectively,
- for gravel thickness of 45 cm by 2.6 %, or 5.8 % respectively.

In increasing the axle load from 22.5 t to 25.0 t or 27.5 t, the increase in deflection is not proportional to the load increase. As compared to the results of half sleeper deflection values measured on models with a half sleeper without a resilient under-sleeper pad, the deflection of a half sleeper with a resilient under-sleeper pad is 6.4 times to 7.1 times greater. Therefore, the deformation the under-sleeper pad has a prominent effect on the deflection of the half sleeper with the under-sleeper pad.

4. The differences in deflection values of the sub-ballast surface in loading the half sleeper without a resilient under-sleeper pad and with a resilient under-sleeper pad are very small (in hundredths of mm). The effect of increasing the gravel thickness and the effect of the resilient under-sleeper pad on the deflection values of the sub-ballast layer cannot be correctly evaluated.
5. The calculated rigidity values of mounting the half sleeper without a resilient under-sleeper pad fluctuate from 51.9 $KN.mm^{-1}$ to 72.3 $kN.mm^{-1}$ while the rigidity values of mounting the half sleeper with a resilient under-sleeper pad fluctuate from 8.1 $kN.mm^{-1}$ to 9.7 $kN^{-1}$. In using the resilient under-sleeper pad the rigidity of the half sleeper mounting is very low (6.4 times to 7.6 times lower than in the case of a half sleeper without the resilient under-sleeper pad).
6. The modulus of deformation of gravel in models with a half sleeper without a resilient under-sleeper pad grows with increased thicknesses of gravel. The results of measurements the moduli of deformation on the ballast surface after loading of half sleeper without under-sleeper pad are displayed in Table 23.

***Table 23: The moduli of deformation on the ballast surface after loading of half sleeper without under-sleeper pad***

| Ballast thickness in cm | Modulus of deformation $E_{V2}$ in MPa | % |
|---|---|---|
| 25 | 57.1 | 100 |
| 35 | 105.1 | 184 |
| 45 | 117.1 | 205 |

The modulus of deformation of gravel in models with a half sleeper with a resilient under-sleeper pad also grows with increased thicknesses of gravel. The results of measurements the moduli of deformation on the ballast surface after loading of half sleeper with under-sleeper pad are displayed in Table 24.

***Table 24: The moduli of deformation on the ballast surface after loading of half sleeper with under-sleeper pad***

| Ballast thickness in cm | Modulus of deformation $E_{V2}$ in MPa | % |
|---|---|---|
| 25 | 64.2 | 100 |
| 35 | 104.7 | 163 |
| 45 | 126.9 | 197 |

7. Overall results of measurement the impact modulus of deformation on the ballast surface under half sleeper without the under-sleeper pad (models B25/SB20/E20, B35/SB20/E20, B45/SB20/E20) and with the under-sleeper pad (models B25/SB20/E20-USP, B35/SB20/E20-USP, B45/SB20/E20-USP) are presented in Table 25.

***Table 25: The static moduli of deformation and the impact moduli of deformation on the ballast surface***

| Ballast thickness in cm | Measurement of $E_{V2}$ and $E_{vd}$ | Static modulus of deformation $E_{V2}$ in MPa | Impact modulus of deformation $E_{vd}$ in MPa | Correlation coefficient $k = E_{V2}/E_{vd}$ | Average $k$ |
|---|---|---|---|---|---|
| 25 | within the building of the model | 57.4 | 40.0 | 1.435 | 1.437 |
| | after loading the sleeper without USP | 57.1 | 43.1 | 1.324 | |
| | after loading the sleeper with USP | 64.2 | 41.3 | 1.554 | |
| 35 | by the building of the model | 90.9 | 58.1 | 1.564 | 1.630 |
| | after loading the sleeper without USP | 105.1 | 60.4 | 1.740 | |
| | after loading the sleeper with USP | 104.7 | 65.9 | 1.588 | |
| 45 | after loading the sleeper without USP | 117.1 | 61.8 | 1.894 | 2.155 |
| | after loading the sleeper with USP | 126.9 | 52.5 | 2.417 | |
| Mean average | | | | | 1.740 |

It results from the Table 25 that correlation coefficient *k* increases with ballast thickness.

8. Repeated usage of the sub-ballast bed of crushed stone mixture and the rail bed layer under the half sleeper in individual models led to accelerated measurement procedures of individual models. The disadvantage, however, was that the results of measurements cannot be correctly mutually compared, as the deflection values, the moduli of deformation and the impact moduli of deformation were measured under different conditions. For example, an increase in the bearing capacity of the crushed stone mixture layer from the initial value of $E_{V2}$ = 37.4 MPa to $E_{V2}$ = 46.1 MPa occurred during the measurements. Analogically, there was a change in the bearing capacity of gravel. From the materials used in model substructure constructions the only material that did not change its bearing capacity were rubber plates with a thickness of 67 mm, simulating the subgrade. Their bearing capacity was determined at the start of experiments as $E_{V2}$ = 20.3 MPa and at the end of measurements as $E_{V2}$ = 19.6 MPa, i.e. by 3.5 % lower.
9. Final evaluation of the results will be made only after the measurements of all model substructure constructions have been completed.

# 12. FEM modelling of the experiments

First task of the project was to evaluate results of the laboratory experiments and expand them to all possible configurations, i.e. for variable thickness of the individual layers. For this purpose a detailed FE model of the experimental box was built and loaded according to the experiments. Three load cases were considered for each configuration a load according to 22.5 t, 25.0 t and 27.5 t. The model is considered as three dimensional elasticity contact problem, where no symmetry is considered. This enables to study more complicated cases (e.g. reinforcement with geosynthetics) where the case may lose it symmetry.

## 12.1 Description of the FE models

The FE model of the experimental box was built using general purpose finite element code ANSYS. The model consists of three layers. The bottom layer represents the rubber plate of two different thicknesses, each corresponding to deformation modulus 20 MPa and 30 MPa respectively. On top of the rubber plate there are two layers of elements representing the sub-ballast layer followed by layer of ballast. The concrete half sleeper is placed resting on the the ballast layer with bottom face covered with contact elements representing the interaction with the underlying layer. The model is depicted in Figure 32.

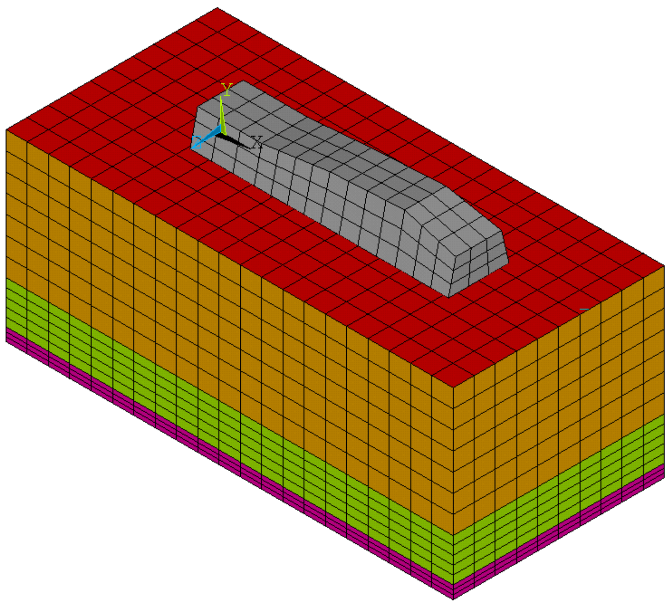

***Figure 32: FE model of the experimental box***

### 12.1.1 Elements used

The geometry of all layers is discredited using is a higher order 3-D 20-node solid element that exhibits quadratic displacement behaviour. The element is defined by 20 nodes having three degrees of freedom per node: translations in the nodal x, y, and z directions.

The interaction between the concrete half sleeper and the layer of gravel is modelled using contact elements. The contact is considered as frictional and is modelled using higher-order contact elements used to represent contact and sliding between 3-D "target" surfaces and a deformable surface, defined by this element. This element is located on the surfaces of 3-D solid elements with mid-side nodes and has the same geometric characteristics as the solid or shell element face with which it is connected to. Contact occurs when the element surface penetrates one of the target segment elements on a specified target surface. Coulomb and shear stress friction is allowed.

### 12.1.2 Material properties

Because of the magnitude of the stresses in considered materials it is possible to use linear elastic material for all the layers. Following material properties were assigned to the materials:

1. concrete sleeper: Young's modulus of elasticity E = 23 000 MPa, Poisson's ratio μ = 0.23
2. ballast: Young's modulus of elasticity E = 80 MPa, Poisson's ratio μ = 0.23
3. sub-ballast layer: Young's modulus of elasticity E = 60 MPa, Poisson's ratio μ = 0.26
4. rubber layer: Young's modulus of elasticity E = 2-10 MPa, Poisson's ratio μ = 0.33

Material properties of the rubber were varied from 2 MPa to 10 MPa as to exclude its influence over the resulting relationship. All materials are considered isotropic.

### 12.1.3 Loading and overview of results

The model is loaded according to the experiments. The top surface of the concrete half sleeper is loaded with load corresponding to axle load of 22.5 kN, 25.0 kN and 27.5 kN. These axle loads correspond force 42 kN, 46.65 kN and 51.30 kN respectively. For each of the load case and for each of the configuration considered, it means for the different thickness of ballast layer (25 cm, 35 cm and 45 cm) the vertical displacements at the selected places are computed and presented in tables showing the correspondence with experimentally derived values. An example of stress distribution in all the layers is presented in Figure 33.

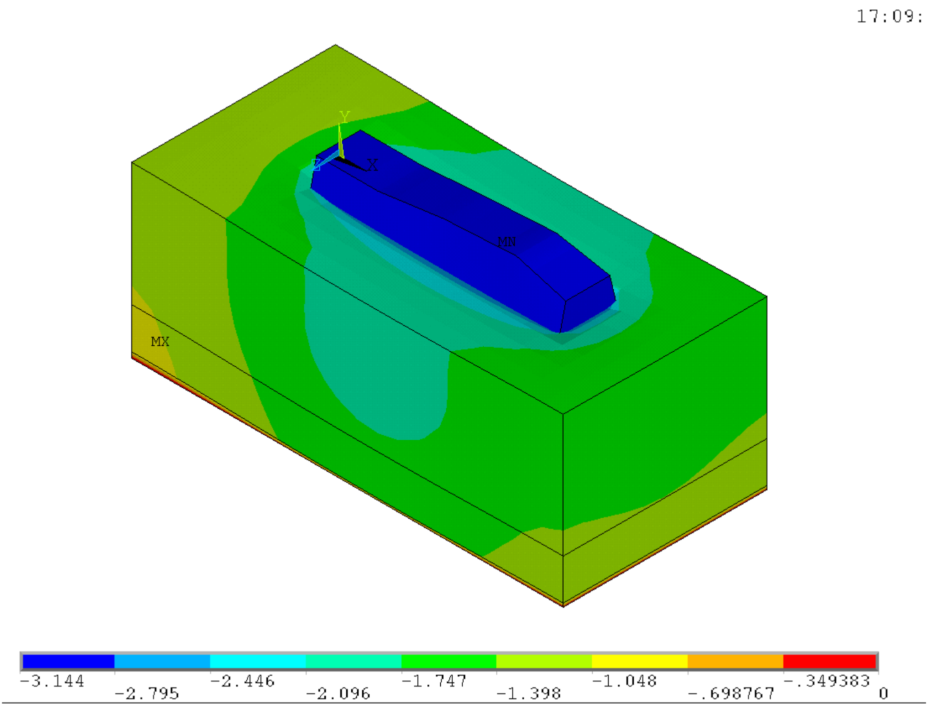


***Figure 33: Third principal stresses distribution in the FE model***

The results from the FEM analysis show good correspondence with expected results and with the deflections measured experimentally. More on the results relevant to the experiments is given in the following section.

### 12.1.4 Relationship between the vertical displacement and principal strains

From the resulting ratios between the principal strain and vertical displacement it is possible to estimate the settlements of the rubber plate in places of measurements. If the principal strains are known and if their relationship with vertical displacement at the same integration point is independent on the material properties then the strain values can be used to calculate the vertical displacements. The ratio between vertical displacement obtained from the FE model and principal strain is used to get the settlement of the rubber plate in the experimental box. Following tables show results for all the load cases considered.

***Table 26: Relationship between the principal strains and vertical displacements for applied load 22.50 tons in case of B25-SB20-E20***

| position | vertical displacement [mm] | principal strain [%] | ratio [-] |
|---|---|---|---|
| 1 | -0.432 | 0.037 | -11.77 |
| 2 | -0.363 | 0.019 | -19.03 |
| 3 | -0.395 | 0.031 | -12.57 |
| 4 | -0.363 | 0.019 | -19.03 |
| 5 | -0.395 | 0.031 | -12.57 |

***Table 27: Relationship between the principal strains and vertical displacements for applied load 22.50 tons in case of B35-SB20-E20***

| position | vertical displacement [mm] | principal strain [%] | ratio [-] |
|---|---|---|---|
| 1 | -0.390 | 0.023 | -17.09 |
| 2 | -0.339 | 0.020 | -21.51 |
| 3 | -0.353 | 0.019 | -18.37 |
| 4 | -0.339 | 0.015 | -21.52 |
| 5 | -0.353 | 0.019 | -18.37 |

***Table 28: Relationship between the principal strains and vertical displacements for applied load 22.50 tons in case of B45-SB20-E20***

| position | vertical displacement [mm] | principal strain [%] | ratio [-] |
|---|---|---|---|
| 1 | -0.360 | 0.016 | -22.25 |
| 2 | -0.320 | 0.013 | -25.20 |
| 3 | -0.327 | 0.012 | -26.84 |
| 4 | -0.322 | 0.013 | -25.20 |
| 5 | -0.327 | 0.012 | -26.84 |

# 13. Vertical displacements calculated vs. measured

In this section, results obtained from the FEM analysis are presented in form of vertical displacements at exact places where the deflections were measured using the deflection meters. The last column in the tables show the deviation between the measured values and values calculated from the FE model.

## 13.1 B25/SB20/E20

The construction of the substructure on which a half of a concrete sleeper B 91 S/1 without the under-sleeper pad was mounted consisted of the following layers:

1. gravel (ballast) 250 mm
2. crushed stone mixture (sub-ballast) 200 mm
3. rubber plates 67 mm

***Table 29: Vertical displacements at places of deflection meters for applied load 22.50 tons***

| Loading [t] | Deflection Meter | Experimental [mm] | Num. Model [mm] | deviation [-] |
|---|---|---|---|---|
| 22.50 | 1 | 0.73 | 0.7468 | 0.08 |
| | 2 | 0.80 | 0.7468 | |
| | 3 | 0.83 | 0.7498 | |
| | 4 | 0.87 | 0.7498 | |
| | average | **0.81** | **0.75** | |
| | A | 0.37 | 0.4876 | 0.10 |
| | B | 0.43 | 0.4876 | |
| | C | 0.42 | 0.4620 | |
| | D | 0.48 | 0.4620 | |
| | average | **0.43** | **0.47** | |

***Table 30: Vertical displacements at places of deflection meters for applied load 25.00 tons***

| Loading [t] | Deflection Meter | Experimental [mm] | Num. Model [mm] | deviation [-] |
|---|---|---|---|---|
| 25.00 | 1 | 0.79 | 0.8257 | 0.05 |
| | 2 | 0.86 | 0.8257 | |
| | 3 | 0.88 | 0.8327 | |
| | 4 | 0.94 | 0.8327 | |
| | average | **0.87** | **0.83** | |
| | A | 0.42 | 0.5414 | 0.10 |
| | B | 0.47 | 0.5414 | |
| | C | 0.45 | 0.5130 | |
| | D | 0.52 | 0.5130 | |
| | average | **0.47** | **0.52** | |

***Table 31: Vertical displacements at places of deflection meters for applied load 27.50 tons***

| Loading [t] | Deflection Meter | Experimental [mm] | Num. Model [mm] | deviation [-] |
|---|---|---|---|---|
| 27.50 | 1 | 0.85 | 0.9079 | 0.03 |
| | 2 | 0.93 | 0.9079 | |
| | 3 | 0.95 | 0.9117 | |
| | 4 | 1.01 | 0.9117 | |
| | average | **0.94** | **0.91** | |
| | A | 0.46 | 0.5952 | 0.13 |
| | B | 0.51 | 0.5952 | |
| | C | 0.49 | 0.5641 | |
| | D | 0.56 | 0.5641 | |
| | average | **0.51** | **0.58** | |

# 13.2 B35/SB20/E20

The construction of the substructure on which a half of a concrete sleeper B 91 S/1 without the under-sleeper pad was mounted consisted of the following layers:

1. gravel (ballast) 350 mm
2. crushed stone mixture (sub-ballast) 200 mm
3. rubber plates 67 mm

***Table 32: Vertical displacements at places of deflection meters for applied load 22.50 tons***

| Loading [t] | Deflection Meter | Experimental [mm] | Num. Model [mm] | deviation [-] |
|---|---|---|---|---|
| 22.50 | 1 | 0.55 | 0.7707 | 0.29 |
| | 2 | 0.55 | 0.7707 | |
| | 3 | 0.65 | 0.7740 | |
| | 4 | 0.65 | 0.7740 | |
| | average | **0.6** | **0.77** | |
| | A | 0.11 | 0.4316 | 1.45 |
| | B | 0.13 | 0.4316 | |
| | C | 0.23 | 0.4011 | |
| | D | 0.21 | 0.4011 | |
| | average | **0.17** | **0.42** | |

***Table 33: Vertical displacements at places of deflection meters for applied load 25.00 tons***

| Loading [t] | Deflection Meter | Experimental [mm] | Num. Model [mm] | deviation [-] |
|---|---|---|---|---|
| 25.00 | 1 | 0.59 | 0.8559 | 0.32 |
| | 2 | 0.60 | 0.8559 | |
| | 3 | 0.71 | 0.8596 | |
| | 4 | 0.69 | 0.8596 | |
| | average | **0.65** | **0.86** | |
| | A | 0.13 | 0.4792 | 1.30 |
| | B | 0.16 | 0.4792 | |
| | C | 0.25 | 0.4455 | |
| | D | 0.24 | 0.4455 | |
| | average | **0.2** | **0.46** | |

***Table 34: Vertical displacements at places of deflection meters for applied load 27.50 tons***

| Loading [t] | Deflection Meter | Experimental [mm] | Num. Model [mm] | deviation [-] |
|---|---|---|---|---|
| 27.50 | 1 | 0.66 | 0.9411 | 0.33 |
| | 2 | 0.67 | 0.9411 | |
| | 3 | 0.76 | 0.9451 | |
| | 4 | 0.75 | 0.9451 | |
| | average | **0.71** | **0.94** | |
| | A | 0.17 | 0.5268 | 1.21 |
| | B | 0.21 | 0.5268 | |
| | C | 0.28 | 0.4898 | |
| | D | 0.26 | 0.4898 | |
| | average | **0.23** | **0.51** | |

## 13.3 B45/SB20/E20

The construction of the substructure on which a half of a concrete sleeper B 91 S/1 without the under-sleeper pad was mounted consisted of the following layers:

1. gravel (ballast) 450 mm
2. crushed stone mixture (sub-ballast) 200 mm
3. rubber plates 67 mm

***Table 35: Vertical displacements at places of deflection meters for applied load 22.50 tons***

| **Loading [t]** | **Deflection Meter** | **Experimental [mm]** | **Num. Model [mm]** | **deviation [-]** |
|---|---|---|---|---|
| 22.50 | 1 | 0.63 | 0.8016 | 0.11 |
| | 2 | 0.67 | 0.8016 | |
| | 3 | 0.77 | 0.8050 | |
| | 4 | 0.79 | 0.8050 | |
| | average | **0.72** | **0.8** | |
| | A | 0.30 | 0.4072 | 0.18 |
| | B | 0.36 | 0.4072 | |
| | C | 0.32 | 0.3792 | |
| | D | 0.33 | 0.3792 | |
| | average | **0.33** | **0.39** | |

***Table 36: Vertical displacements at places of deflection meters for applied load 25.00 tons***

| **Loading [t]** | **Deflection Meter** | **Experimental [mm]** | **Num. Model [mm]** | **deviation [-]** |
|---|---|---|---|---|
| 25.00 | 1 | 0.69 | 0.8902 | 0.14 |
| | 2 | 0.72 | 0.8902 | |
| | 3 | 0.84 | 0.8940 | |
| | 4 | 0.86 | 0.8940 | |
| | average | **0.78** | **0.89** | |
| | A | 0.34 | 0.4522 | 0.22 |
| | B | 0.40 | 0.4522 | |
| | C | 0.35 | 0.4211 | |
| | D | 0.36 | 0.4211 | |
| | average | **0.36** | **0.44** | |

***Table 37: Vertical displacements at places of deflection meters for applied load 27.50 tons***

| **Loading [t]** | **Deflection Meter** | **Experimental [mm]** | **Num. Model [mm]** | **deviation [-]** |
|---|---|---|---|---|
| 27.50 | 1 | 0.76 | 0.9788 | 0.14 |
| | 2 | 0.79 | 0.9788 | |
| | 3 | 0.93 | 0.9830 | |
| | 4 | 0.95 | 0.9830 | |
| | average | **0.86** | **0.98** | |
| | A | 0.38 | 0.4972 | 0.19 |
| | B | 0.45 | 0.4972 | |
| | C | 0.38 | 0.4629 | |
| | D | 0.41 | 0.4629 | |
| | average | **0.41** | **0.48** | |

# 13.4 Conclusions

Numerical models showed good correspondence with the experimental results for all cases (average standard deviation is 16.7 %), except for the case of ballast thickness 350 mm. The discrepancy was probably caused by an error in measurement of the sleeper deflections. The calculated displacements at the ballast sub-ballast interface were in good agreement with experimental values even in the case of ballast thickness 350 mm (average standard deviation less than 15.6 %).

The possibilities of the FE model are not limited to verification of the experimental results in terms of trends of the measured quantities but it is also possible to expand the results for all possible configurations. This enables to draw design graphs for different configurations of the substructure and also to study the reinforcing effects of e.g. geogrids and cement layers.

# 14. Design graphs for single layer construction

First task of the project was to evaluate results of the laboratory experiments and expand them to all possible configurations, i.e. for variable thickness of the individual layers. Single layer construction type consisting of one sub-ballast layer of variable thickness is considered, see Figure 34.

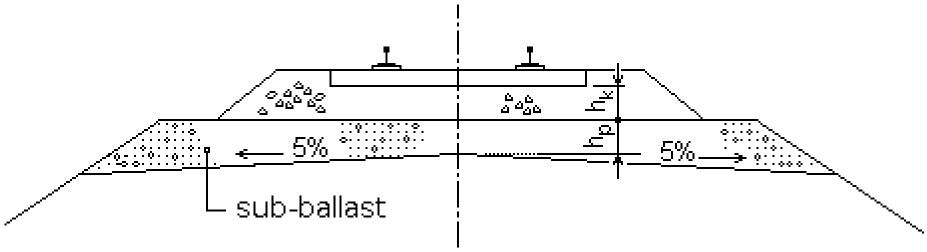


***Figure 34: Single layer construction of substructure***

## 14.1 Description of the FE models

The models used in the numerical study are all plane strain models. The geometry respects the real geometry of the experimental box. The bearing capacity of the single layer construction model is evaluated using 0.2 MPa load. The surface is loaded by circular plate with 0.3 m diameter.

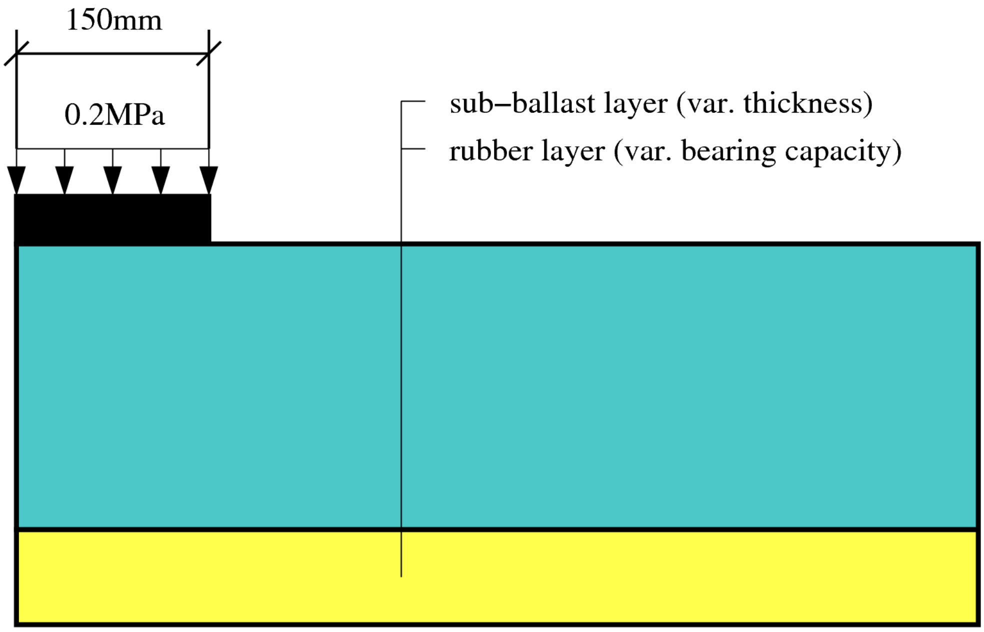


***Figure 35: Scheme of the mathematical model (single layer construction)***

The domains were discretized using eight-node quadratic plane strain elements. The element has 16 degrees of freedom in total, two translational DOFs in each node. The finite element mesh of the problem is shown in Figure 36. The model includes three different material models for the steel plate, sub-ballast layer and rubber (foundation). For each of the models an iterative approach is taken to find thickness of the sub-ballast layer such the required bearing capacity of the layered system is obtained.

Values of the Young's modulus were calculated from the modulae of deformation and Poisson's ratio for the case of plain strain given by boundary conditions $\varepsilon_z = 0$. The equation describing compression of soil is simply written as

$$E_{oed} = \frac{\sigma_z}{\varepsilon_z} = \frac{h}{\Delta h}\sigma_z$$

Where $E_{oed}$ is edometrical modulus, $\sigma_z$ is stress in z-direction, $\varepsilon_z$ is strain in z-direction and $\Delta h$ is value of vertical deflection. Then relation between $E_{oed}$ and Young's modulus of elasticity $E$ is derived from the extended Hook’s law. The relationship can be written as follows:

$$E = E_{oed}\left(1 - \frac{2v^2}{1-v}\right)$$

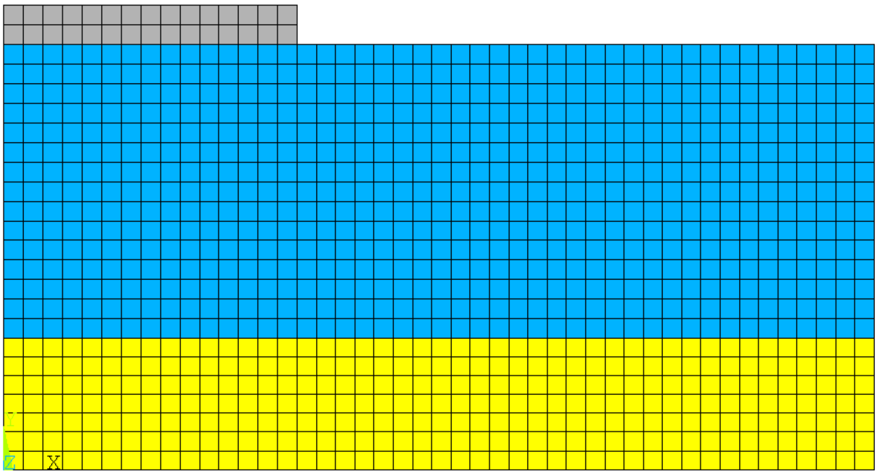

*Figure 36: Finite element mesh – single layer model (plain strain)*

## 14.2 Results

The results of the numerical analyses were developed into a set of design graphs. The graphs are suitable for easy use and therefore for individual required modulus of deformation one graph is plotted. With the help of the nomograms it is easy to find appropriate thickness of the sub-ballast layer for given modulus of deformation of the subgrade and given required modulus of deformation. With the help of the FE models it is possible to list other important values, e.g. principal strains and stresses or displacements in the respective layers. Following figure shows vertical displacements in the FE model.

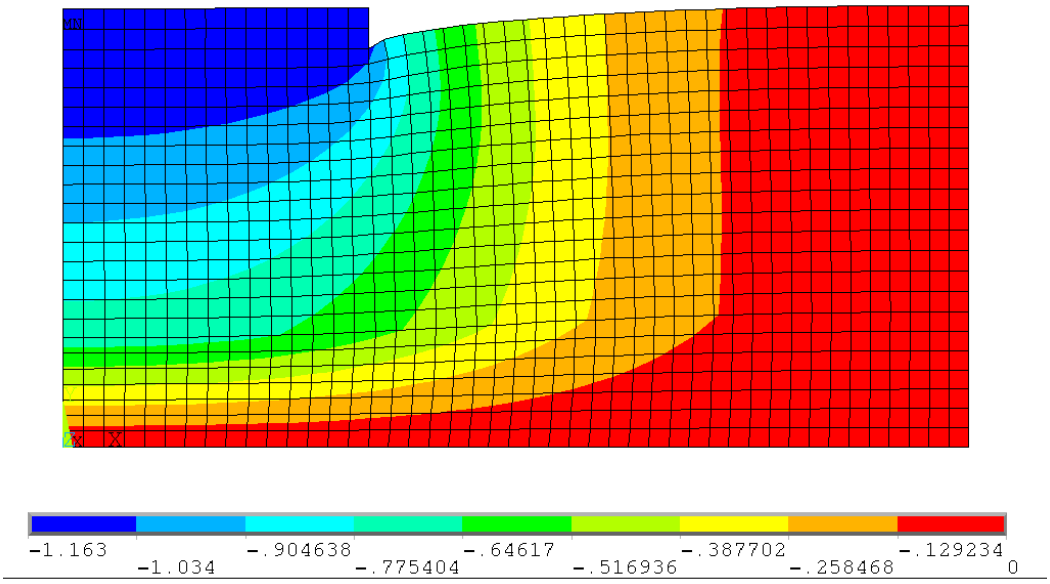


*Fig. 14.1 Vertical displacements in the plain strain model*

## 14.2.1 Design graph for required modulus of deformation E = 20 MPa

Following figure shows the first design-graph for required modulus of deformation E = 20 MPa. Horizontal axis lists modulus of deformation of the existing subgrade and for each modulus of deformation of the subballast a design curve is plotted. Vertical axis lists subballast thickness required to achieve specified modulus of deformation.

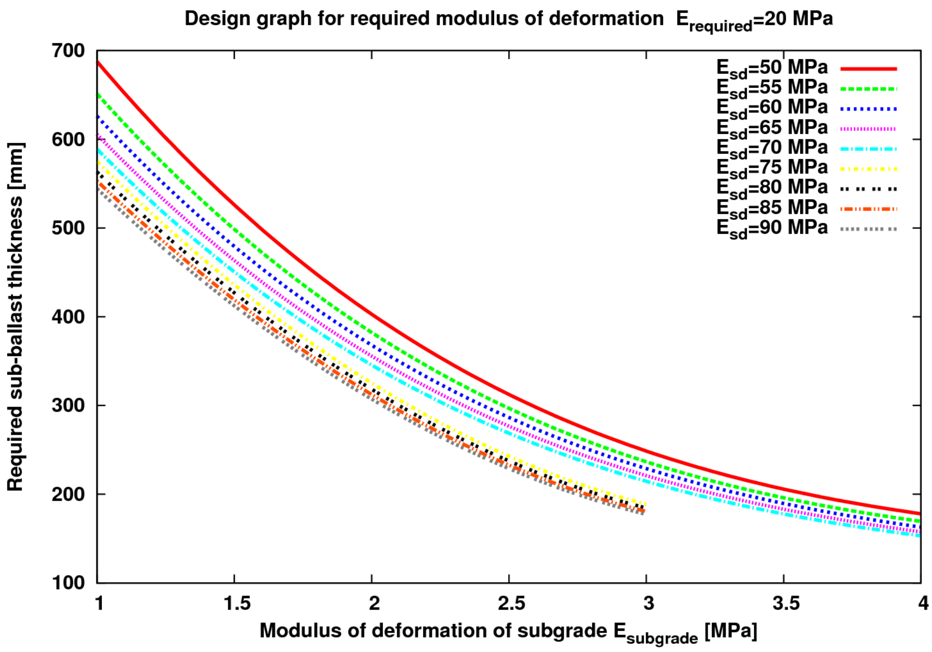


***Figure 37: Design graph -required modulus of deformation E = 20 MPa***

All design graphs were evaluated for the required modulus of deformation stepped in 5 MPa increments. In the report design graphs are listed for 10 MPa increment. The smallest value of required modulus of deformation was considered 20 MPa. The largest taken into account was 90 MPa. The moduli of deformation of the sub-ballast were stepped in 5 MPa increments.

### 14.2.2 Design graph for required modulus of deformation E = 30 MPa

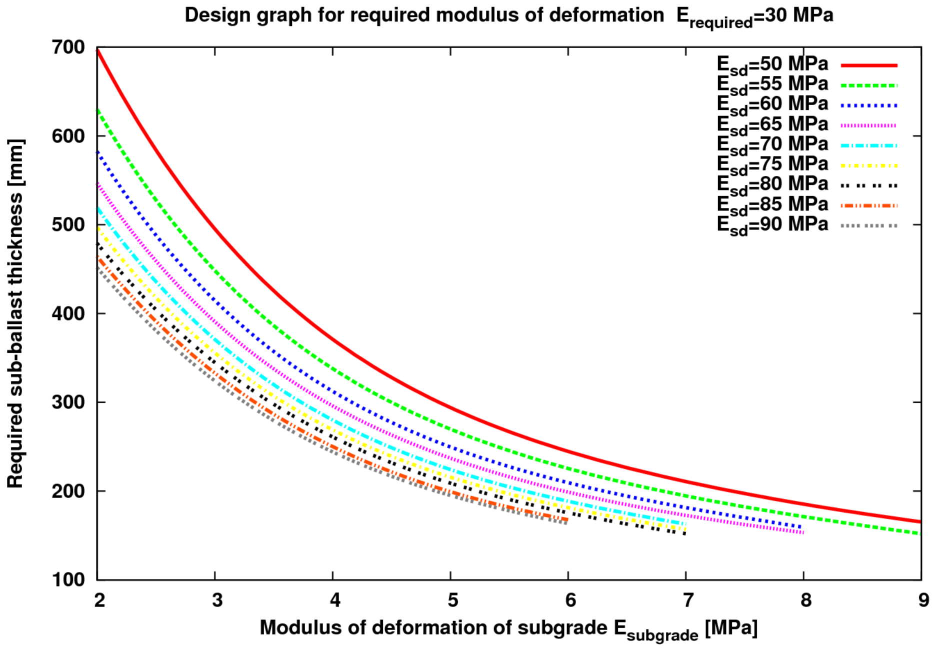


***Figure 38: Design graph -required modulus of deformation E = 30 MPa***

### 14.2.3 Design graph for required modulus of deformation E = 40 MPa

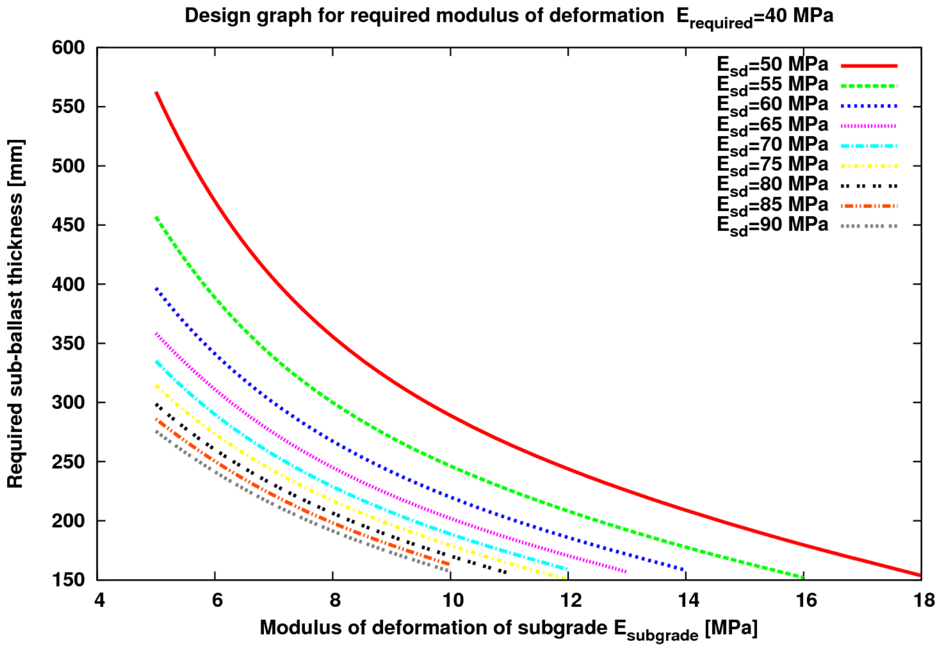


***Figure 39: Design graph -required modulus of deformation E = 40 MPa***

### 14.2.4 Design graph for required modulus of deformation E = 50 MPa

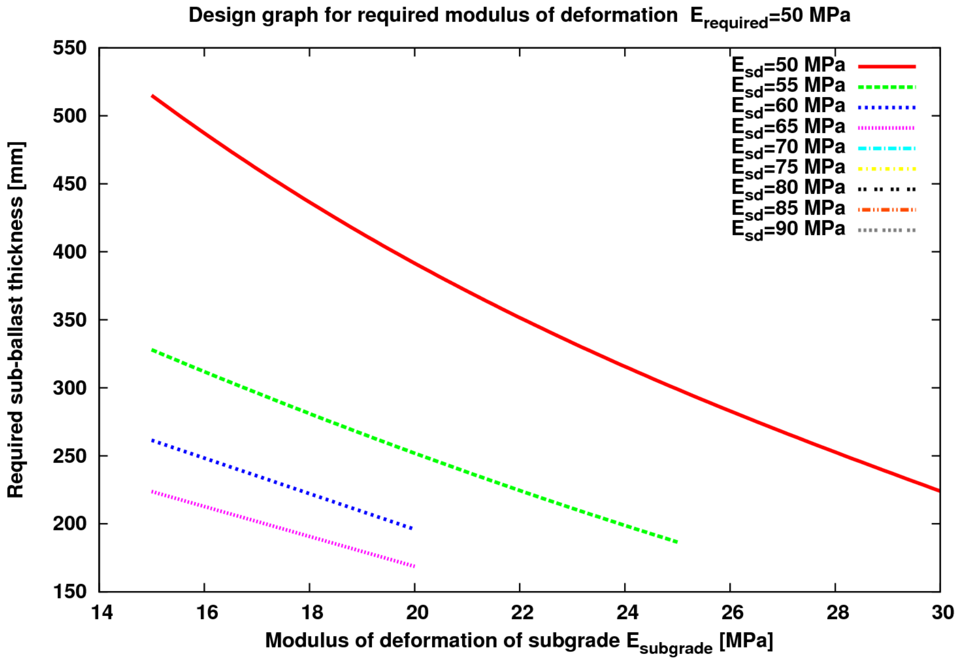


***Figure 40: Design graph -required modulus of deformation E = 50 MPa***

### 14.2.5 Design graph for required modulus of deformation E = 60 MPa

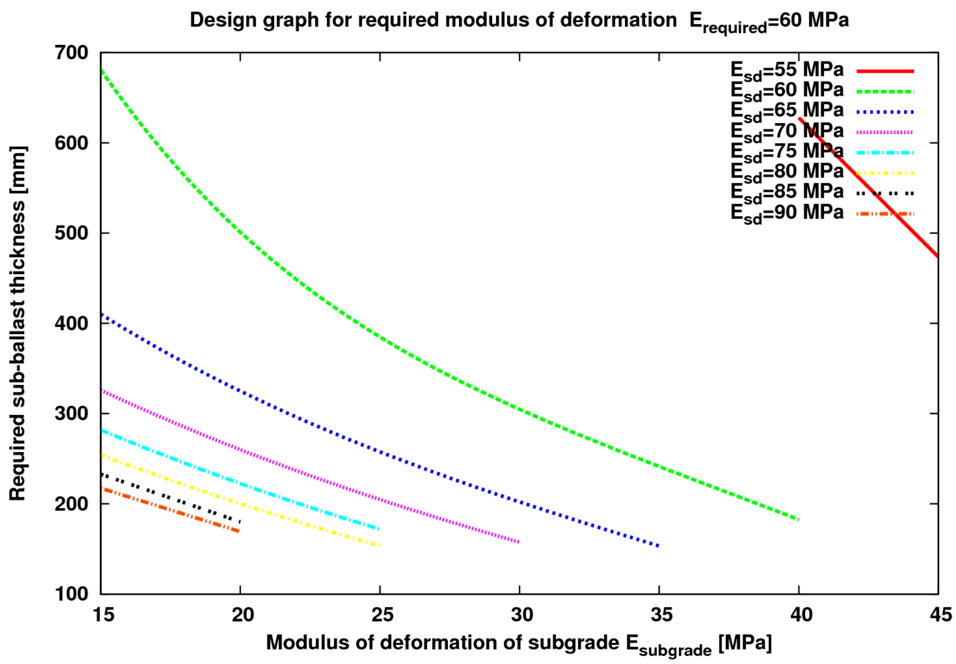


***Figure 41: Design graph -required modulus of deformation E = 60 MPa***

### 14.2.6 Design graph for required modulus of deformation E = 70 MPa

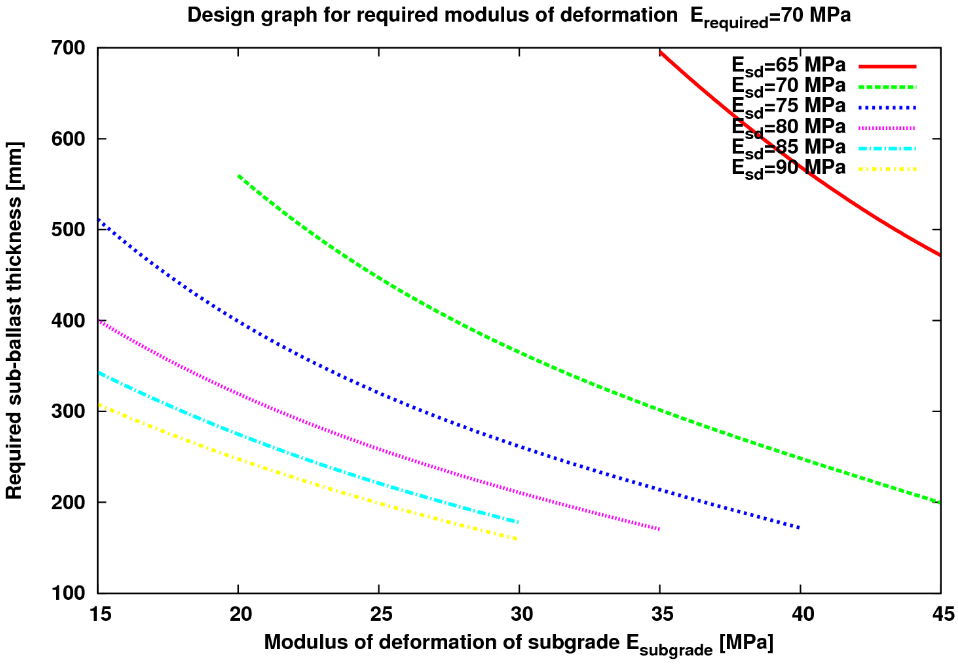


***Figure 42: Design graph -required modulus of deformation E = 70 MPa***

### 14.2.7 Design graph for required modulus of deformation E = 80 MPa

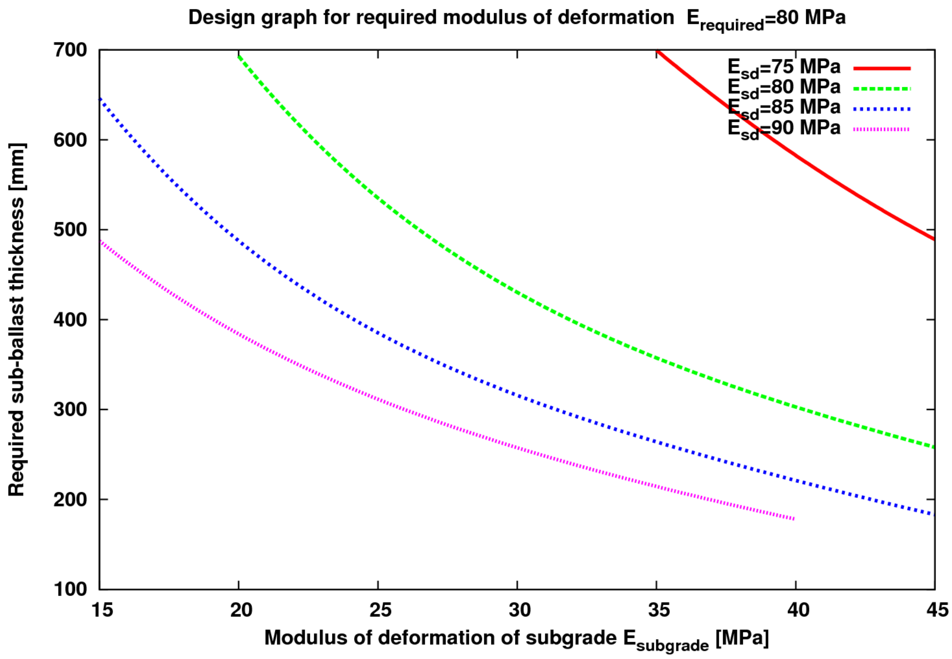


***Figure 43: Design graph -required modulus of deformation E = 80 MPa***

# 15. Design graphs for two-layer construction

The objective of this part of the work was to extend the FE models to two-layer construction, where the layers are distinguished by their material properties and thicknesses. Evaluation of the design graphs is similar to the single layer construction. Apart from the design graphs, the purpose of these models is to enable for future mathematical modelling of reinforcing effects by inclusion of geosynthetics between the two layers or to simulate reinforcing effects of lime or cement layer.

## 15.1 Description of the FE models

Again, bearing capacity of the two-layer construction model is evaluated using 0.2 MPa load. The surface is loaded by circular plate with 0.3 m diameter as seen in Figure 44.

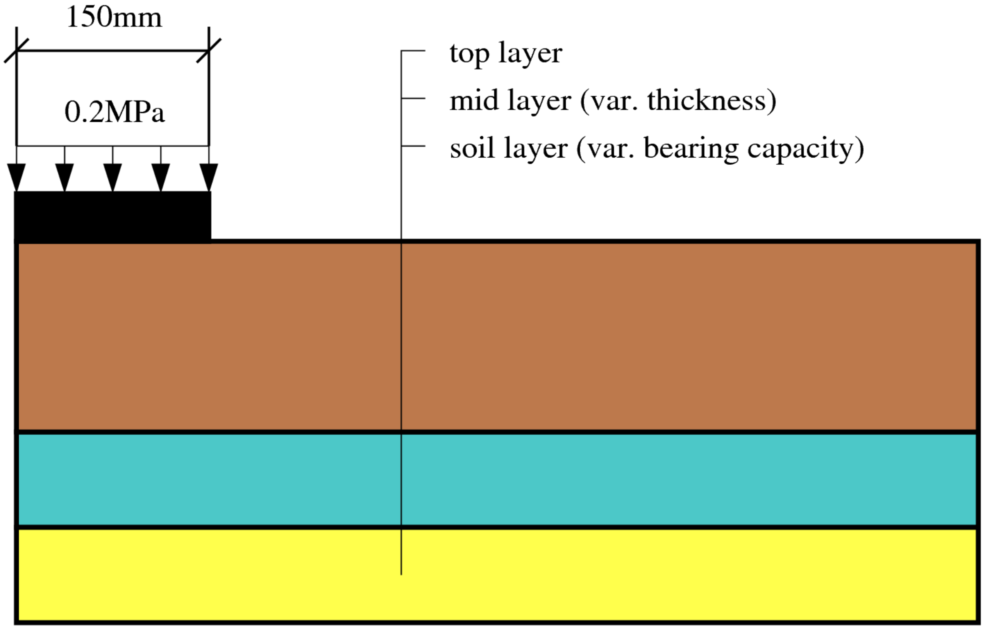


***Figure 44: Scheme of the mathematical model (two-layer construction)***

## 15.2 Results

Results are again presented in terms of easy-to-use design graphs. In the FE models, the thickness of the top layer is held constant, but it is easy to present results also for variable thickness of the upper layer. This will be presented in terms of design tables but it is out of the scope of the report. Presented design graphs are for the required modulus of deformation in the interval from 50 MPa to 90 MPa.

### 15.2.1 Design graphs for required modulus of deformation E = 60 MPa

Following figure shows the first design-graph for required modulus of deformation E = 60 MPa. Horizontal axis lists modulus of deformation of the existing subgrade and for each modulus of deformation of the subballast a design curve is plotted. Vertical axis lists subballast thickness required to achieve specified modulus of deformation. For each required modulus of deformation three solutions for different thickness of the top layer (250, 350 and 450 mm) were found. In some graphs only few curves for selected moduli of deformation of sub-ballast are plotted, because of no solution in specified interval of modulus of deformation of the subgrade.

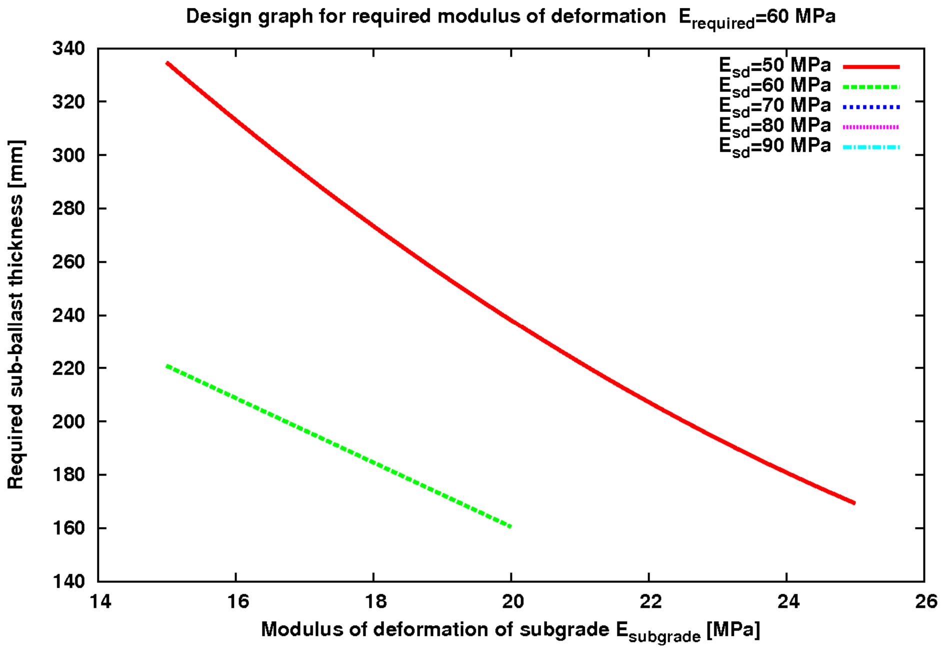


***Figure 45: Design graph - required modulus of deformation E = 60 MPa, thickness of the top layer 25 mm***

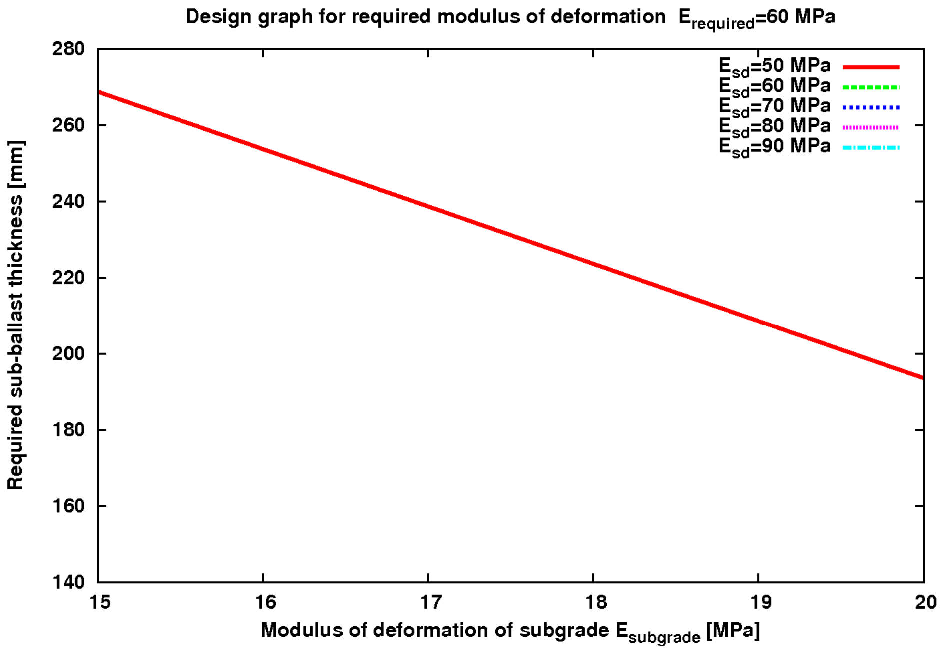


***Figure 46: Design graph - required modulus of deformation E = 60 MPa, thickness of the top layer 35 mm***

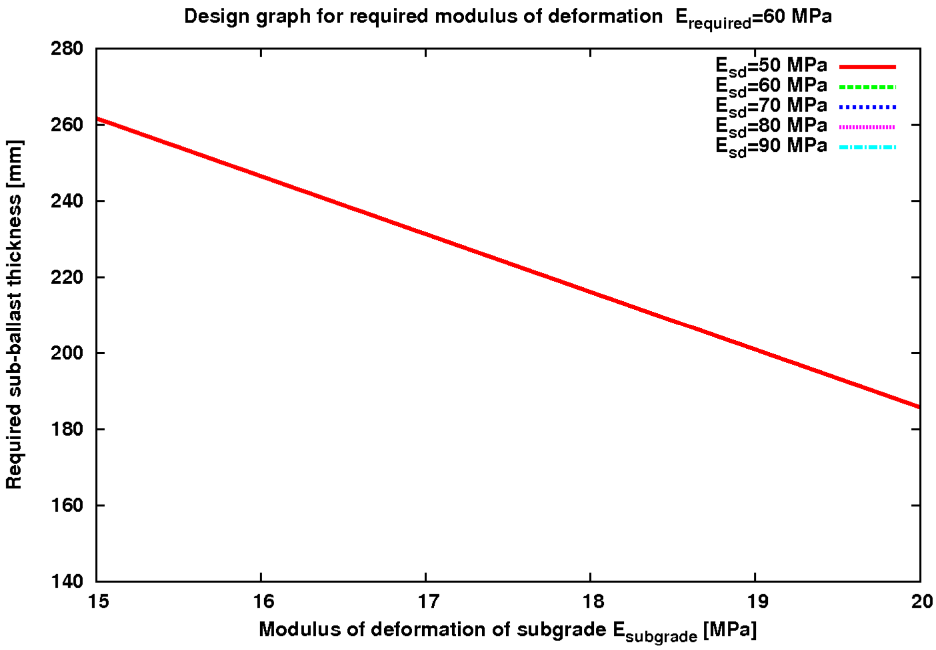


***Figure 47: Design graph - required modulus of deformation E = 60 MPa, thickness of the top layer 45 mm***

## 15.2.2 Design graphs for required modulus of deformation E = 70 MPa

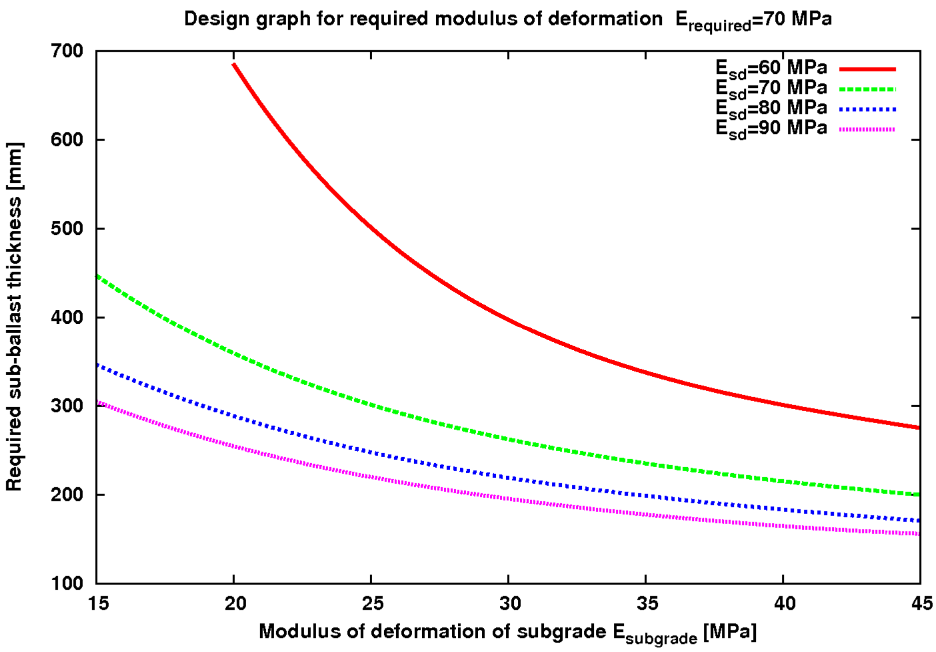


***Figure 48: Design graph - required modulus of deformation E = 70 MPa, thickness of top layer 25 mm***

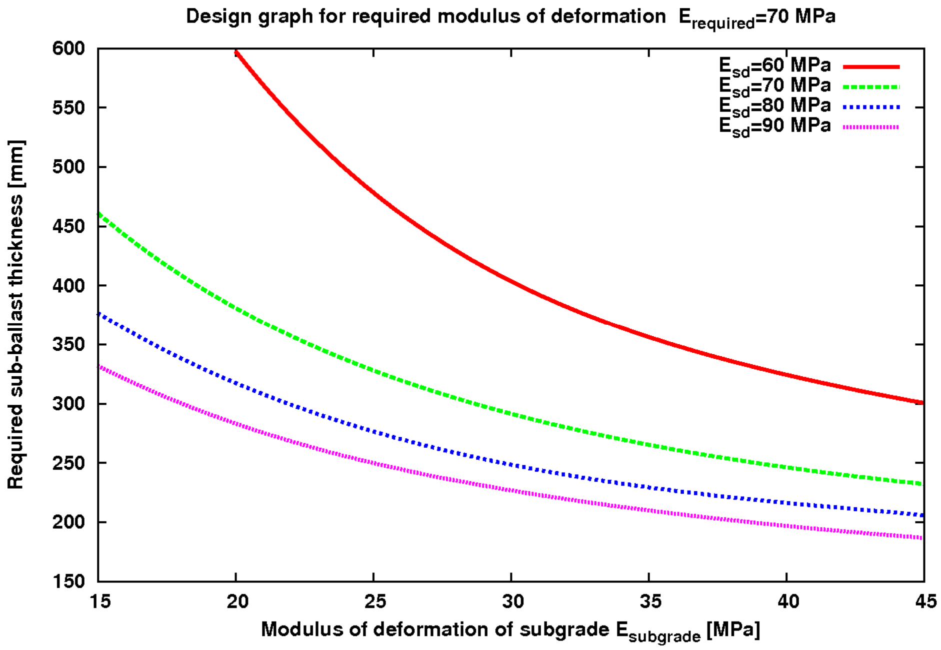


***Figure 49: Design graph - required modulus of deformation E = 70 MPa, thickness of top layer 35 mm***

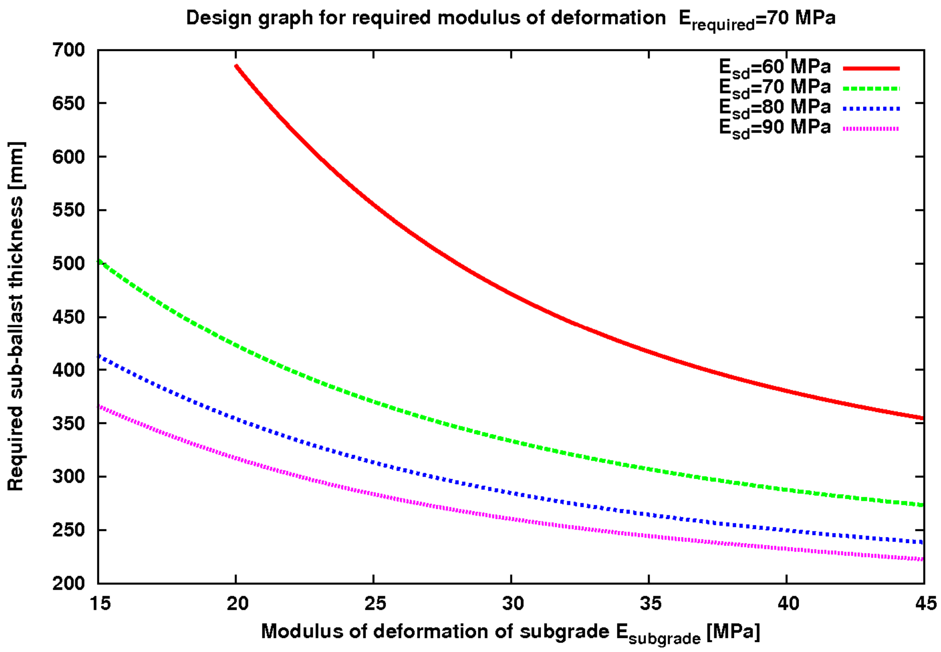


***Figure 50: Design graph - required modulus of deformation E = 70 MPa, thickness of top layer 45 mm***

### 15.2.3 Design graphs for required modulus of deformation E = 80 MPa

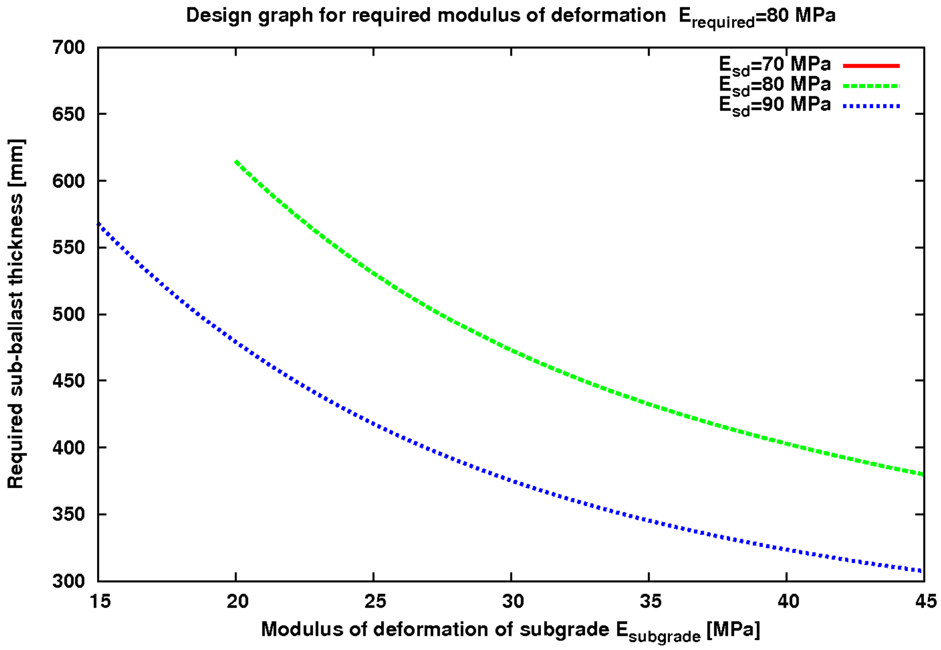


***Figure 51: Design graph - required modulus of deformation E = 80 MPa, thickness of the top layer 25 cm***

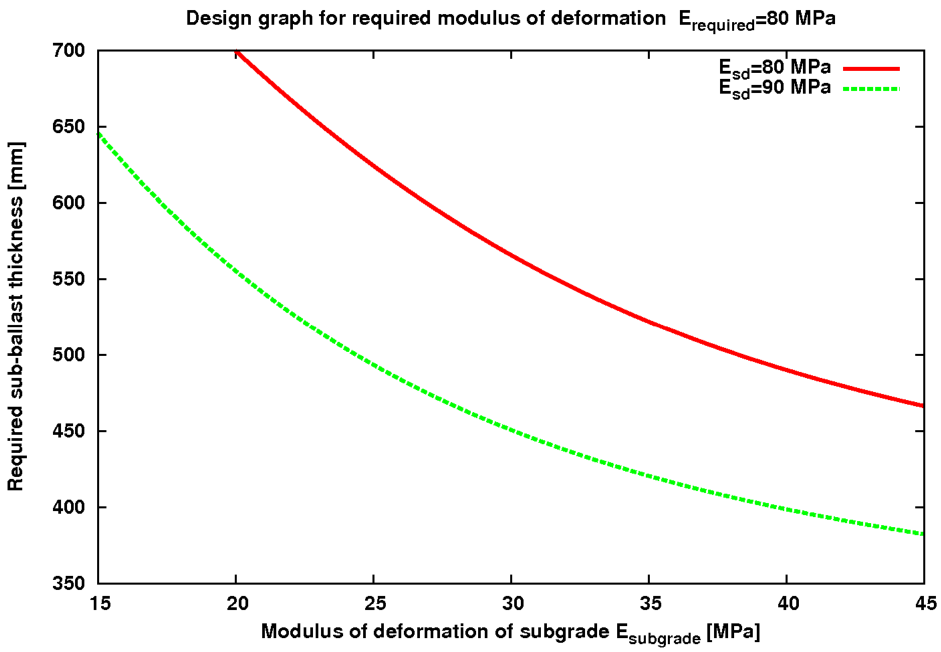


***Figure 52: Design graph - required modulus of deformation E = 80 MPa, thickness of the top layer 35 cm***

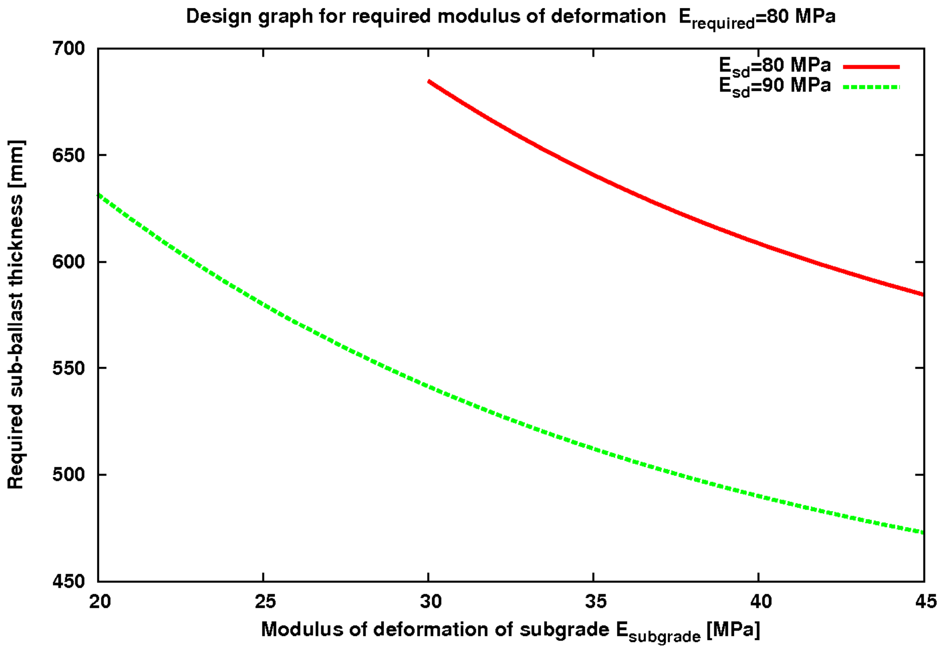


***Figure 53: Design graph - required modulus of deformation E = 80 MPa, thickness of the top layer 45 cm***

# 16. Conclusions of numerical modelling

Presented finite element models are used to find unifying methodology to design railway subbase. The approach is easily extensible in such a way, that various reinforcing means can be included. Further implementation of single or multiple layers of geosynthetics will be undertaken as well as use of lime or cement layers will be explored. For each of the possible design, bearing capacity will be evaluated. This approach enables to find an optimal solution to the specific problem given.

Three dimensional, fully parametric FE models are being evaluated, one of them shown in Figure 54. These models enable to study behaviour of the complex system under various loading conditions.

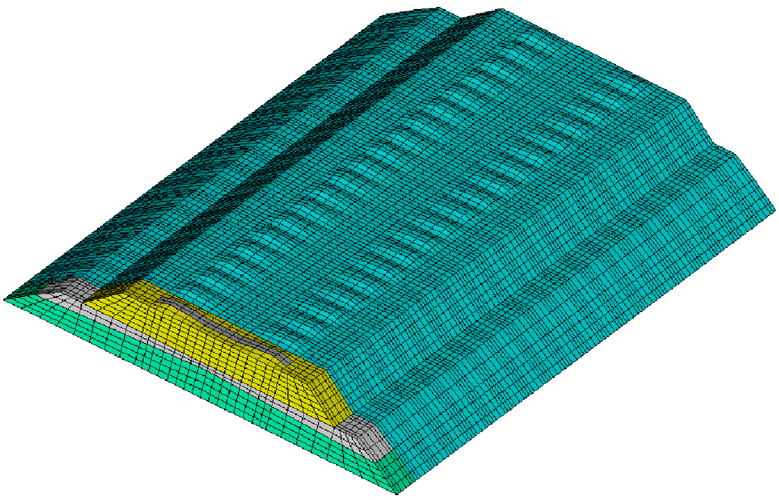

***Figure 54: 3-D FE model of the track bed and single layer construction***

Inclusion of the geosynthetics is studied on similar FE models, scheme of such a model is given in Figure 55. These models will be reported as a part of other deliverable.

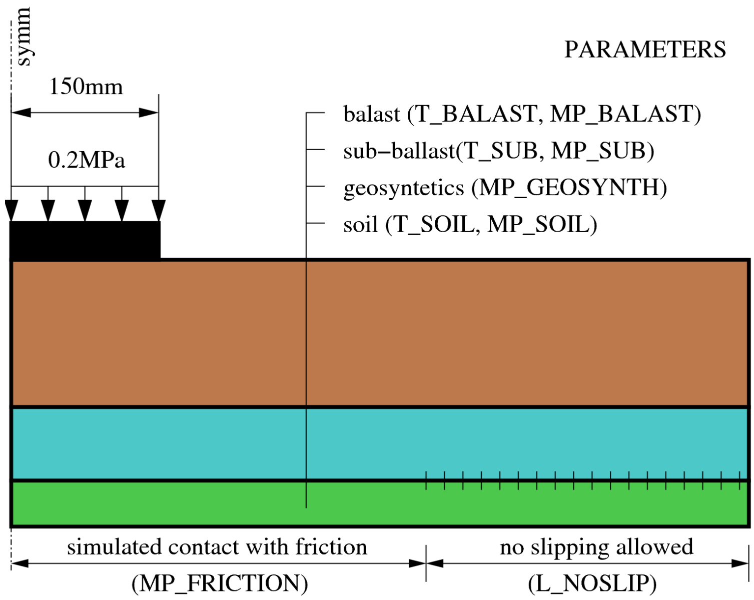


***Figure 55: Scheme of the FE model with geosynthetics***

# Bibliography

1. DIN 18 134 Plattendruckversuch. Deutsches Institut für Normen e. V., 1993
2. TP BF-StB Teil B 8.3 Dynamischer Plattendruckversuch mit Leichtem Fallgewichtsgerät, 2003
3. ČSN 73 6192 Impact Load Tests of Roads and Underlays, 1996
4. Göbel, C. – Lieberenz, K.: Handbuch Erdbauwerke der Bahnen. Eurailpress, Hamburg, 2004, ISBN 3-7771-0317-9
5. Selig, E. T. - Waters, J. M.: Track Geotechnology and Substructure Management. Thomas Telford Services Ltd, London, 1994, ISBN 0-7277-2013-9
6. Esveld, C. Modern Railway Track, 2nd ed. MRT Productions, Zaltbommel, 2001, ISBN 90-800324-3-3
7. Suiker, A. S. J.: The Mechanical Behaviour of Ballasted Railway Tracks. Ph D Thesis, Delft University of Technology, DUP Science, June 2002, 237 p. ISBN 90-407-2307-9
8. Führer, G.: Oberbauberechnung, Transpress, Berlin, 1978
9. Lichtberger, B.: Track Compendium, Eurail Press, Hamburg, 2005, ISBN 3-7771-0320-9
10. Finite Element Method- Volume 1- The Basis, Zienkiewicz, O. C. and Taylor, R. L., 2000
11. Finite Element Method- Volume 2- Solid Mechanics, Zienkiewicz, O. C. and Taylor, R. L., 2000
12. Non-linear Finite Element Analysis of Solids and Structures, Vol 1 , Crisfield, M. A., 1997
13. Non-linear Finite Element Analysis of Solids and Structures, Vol 2 , Crisfield, M. A., 1997